

# Mitochondrial fission factor (MFF) is a critical regulator of peroxisome maturation

Josiah B. Passmore<sup>1</sup>, Luis F. Godinho<sup>1</sup>, Sacha Ferdinandusse<sup>2</sup>, Celien Lismont<sup>3</sup>, Yunhong Wang<sup>4</sup>, Christian Hacker<sup>1</sup>, Markus Islinger<sup>4</sup>, Marc Fransen<sup>3</sup>, David M. Richards<sup>5</sup>, Peter Freisinger<sup>6</sup>, Michael Schrader<sup>1,\*</sup>

<sup>1</sup>Biosciences, University of Exeter, Exeter, UK

<sup>2</sup>Laboratory Genetic Metabolic Diseases, Amsterdam University Medical Centre, University of Amsterdam, The Netherlands

<sup>3</sup>Department of Cellular and Molecular Medicine, KU Leuven, Leuven, Belgium

<sup>4</sup>Institute of Neuroanatomy, Center for Biomedicine & Medical Technology Mannheim, Medical Faculty Mannheim, University of Heidelberg, Mannheim, Germany

<sup>5</sup>LSI, University of Exeter, Exeter, UK

<sup>6</sup>Department of Pediatrics, Kreiskliniken Reutlingen, Reutlingen, Germany

\*Address all correspondence to Michael Schrader, College of Life and Environmental Sciences, Biosciences, University of Exeter, Geoffrey Pope Building, Stocker Road, Exeter EX4 4QD, UK

E-mail: [m.schrader@exeter.ac.uk](mailto:m.schrader@exeter.ac.uk) Telephone: +44 (0) 1392 725850

**Running title:** Peroxisome abnormalities in MFF-deficient cells

**Keywords:** Peroxisomes, mitochondria, organelle division, MFF, PEX14, redox homeostasis, pexophagy

**Abbreviations:** ACOX1, acyl-CoA oxidase 1; PBD, peroxisome biogenesis disorder; PED, single peroxisomal enzyme deficiency; DRP1, dynamin-related protein 1; ER, endoplasmic reticulum; FIS1, mitochondrial fission 1 protein; MFF, Mitochondrial fission factor; ROS, reactive oxygen species; PTS, peroxisome targeting signal; VLCFA, very-long-chain fatty acid.

## 29 **Abstract**

30 Peroxisomes are highly dynamic subcellular compartments with important functions in lipid and ROS  
 31 metabolism. Impaired peroxisomal function can lead to severe metabolic disorders with developmental  
 32 defects and neurological abnormalities. Recently, a new group of disorders has been identified,  
 33 characterised by defects in the membrane dynamics and division of peroxisomes rather than by loss of  
 34 metabolic functions. However, the contribution of impaired peroxisome plasticity to the  
 35 pathophysiology of those disorders is not well understood. Mitochondrial fission factor (MFF) is a key  
 36 component of both the peroxisomal and mitochondrial division machinery. Patients with MFF  
 37 deficiency present with developmental and neurological abnormalities. Peroxisomes (and mitochondria)  
 38 in patient fibroblasts are highly elongated as a result of impaired organelle division. The majority of  
 39 studies into MFF-deficiency have focused on mitochondrial dysfunction, but the contribution of  
 40 peroxisomal alterations to the pathophysiology is largely unknown. Here, we show that MFF deficiency  
 41 does not cause alterations to overall peroxisomal biochemical function. However, loss of MFF results  
 42 in reduced import-competency of the peroxisomal compartment and leads to the accumulation of pre-  
 43 peroxisomal membrane structures. We show that peroxisomes in MFF-deficient cells display alterations  
 44 in peroxisomal redox state and intra-peroxisomal pH as well as altered distribution in neuronal cells.  
 45 Removal of elongated peroxisomes through induction of autophagic processes is not impaired. A  
 46 mathematical model describing key processes involved in peroxisome dynamics sheds further light into  
 47 the physical processes disturbed in MFF-deficient cells. The consequences of our findings for the  
 48 pathophysiology of MFF-deficiency and related disorders with impaired peroxisome plasticity are  
 49 discussed.

# 1. Introduction

Peroxisomes are highly dynamic membrane-bound organelles with key functions in cellular lipid and ROS metabolism. Defects in peroxisome biogenesis and metabolic function can result in severe disorders with developmental defects and neurological abnormalities (Dorninger et al. 2017; Wanders 2018). Peroxisome biogenesis disorders (PBDs) result from mutations in *PEX* genes, which encode proteins essential for peroxisomal membrane biogenesis and matrix protein import. PBDs, such as Zellweger Spectrum disorders, are usually characterised by a loss of functional peroxisomes. This impacts on multiple metabolic pathways (e.g., peroxisomal  $\alpha$ - and  $\beta$ -oxidation of fatty acids, and the synthesis of ether-phospholipids, which are abundantly present in myelin sheaths) and results in various patient phenotypes and symptoms (Braverman et al. 2016). Peroxisomal single enzyme deficiencies (PEDs) on the other hand are caused by mutations in genes encoding a specific peroxisomal enzyme/protein and usually affect one metabolic pathway or function. The most prominent example is X-linked adrenoleukodystrophy, which is caused by mutations in the *ABCD1* gene, encoding a peroxisomal ABC transporter required for the import of very-long-chain fatty acids (VLCFAs) into the organelle (Raymond et al. 1993). In addition to PBDs and PEDs, a third group of disorders has been identified, which is characterised by defects in the membrane dynamics and division of peroxisomes rather than by loss of metabolic functions (Waterham et al. 2007; Shamseldin et al. 2012; Ebberink et al. 2012; Koch et al. 2016).

Peroxisomes can form and multiply by growth and division, a defined multistep pathway involving membrane elongation of existing peroxisomes, constriction, and membrane fission (Schrader et al. 2016). In mammals, this involves the coordinated interplay of key membrane-shaping and fission proteins such as PEX11 $\beta$ , FIS1, MFF, and DRP1 (encoded by the *DNML1* gene) (Schrader et al. 2016). The peroxisomal membrane protein PEX11 $\beta$  is involved in several steps of peroxisomal growth and division: membrane deformation to facilitate elongation (Delille et al. 2010; Opaliński et al. 2011), recruitment of the division factors MFF and FIS1 to constriction sites (Koch et al. 2005; Koch and Brocard 2012; Itoyama et al. 2013), and activation of the fission GTPase DRP1 (Williams et al. 2015). The tail-anchored membrane proteins MFF and FIS1 act as adaptor proteins for the recruitment of DRP1 to the peroxisomal membrane and interact with PEX11 $\beta$  (Schrader et al. 2016). With the exception of PEX11 $\beta$ , all proteins involved in peroxisome growth and division identified so far are also key mitochondrial division factors. FIS1 and MFF are dually targeted to both peroxisomes and mitochondria, and also recruit DRP1 to the mitochondrial outer membrane (Koch et al. 2005; Gandre-Babbe and van der Bliek 2008; Costello et al. 2017a, 2018). Mitochondria also possess the adaptor proteins MiD49 and MiD51, which are specific to mitochondria and can recruit DRP1 independent of FIS1 and MFF (Palmer et al. 2013). GDAP1 is another tail-anchored membrane protein shared by mitochondria and peroxisomes, which influences organelle fission in an MFF- and DRP1-dependent manner in neurons (Huber et al. 2013). Recently, also MIRO1, a tail-anchored membrane adaptor for the microtubule-dependent motor protein kinesin, has been shown to localise to mitochondria and peroxisomes and to contribute to peroxisomal motility and membrane dynamics (Castro et al. 2018; Okumoto et al. 2018).

Patients with mutations in DRP1/DNML1, PEX11 $\beta$ , or MFF have been identified and often present with neurological abnormalities (Waterham et al. 2007; Shamseldin et al. 2012; Ebberink et al. 2012; Costello et al. 2018). Loss of DRP1 or MFF function leads to a block in mitochondrial and peroxisomal fission resulting in highly elongated organelles with impaired dynamics. However, the metabolic functions of both peroxisomes and mitochondria are typically not or only slightly altered, indicating that changes in organelle dynamics and plasticity are the main contributors to the pathophysiology of the disease (Waterham et al. 2007; Shamseldin et al. 2012; Koch et al. 2016; Yoon et al. 2016; Vanstone et al. 2016; Nasca et al. 2016, 2018; Gerber et al. 2017; Ladds et al. 2018).

MFF deficiency displays with developmental delay, peripheral neuropathy, optic atrophy, and Leigh-like encephalopathy (Shamseldin et al. 2012; Koch et al. 2016; Nasca et al. 2018). The mitochondria in MFF-deficient patient fibroblasts show no significant alteration in oxidative phosphorylation or mtDNA (Koch et al. 2016; Nasca et al. 2018). Likewise, loss of MFF did not significantly alter the mitochondrial membrane potential, ATP levels or the redox potential of the mitochondrial matrix in neuronal cells (Lewis et al. 2018). While the majority of studies into MFF-deficiency have focused on mitochondrial dysfunction, the contribution of peroxisomal alterations to the pathophysiology is largely unknown. Similarly to DRP1 and PEX11 $\beta$  patients, it appears that peroxisomal metabolic function is unaltered (Koch et al. 2016; Nasca et al. 2018), with the only known peroxisome dysfunction being hyperelongation. In this study, we assess the extent to which peroxisomal functions and properties are altered in MFF-deficient cells, giving further insight into the pathophysiological consequences of loss-of-function of MFF. We show that loss of MFF impacts on the distribution of peroxisomal marker proteins and causes the accumulation of pre-peroxisomal membrane structures. Furthermore, peroxisomes in MFF-deficient cells display alterations in peroxisomal redox state and intra-peroxisomal pH as well as altered peroxisome distribution in neuronal cells. Interestingly, elongated peroxisomes in MFF-deficient cells are not fully static, and their dynamics can be modulated, e.g. through the induction of autophagic processes. The consequences of our findings for the understanding of the pathophysiology of MFF-deficiency and related disorders with impaired peroxisome plasticity are discussed.

## 2. Materials and Methods

### 2.1. Plasmids, Antibodies and siRNAs

The plasmids and antibodies used in this study are detailed in Tables S1 and S2, respectively. PEX14 siRNA (GAACUCAAGUCCGAAAUUA) (Lee et al. 2017) and MFF siRNA (GACCAGCAGAUCUUGACCU) (Long et al. 2013) were generated by Eurofins as 21-mer siRNAs with 3' dTdT overhangs. siGENOME Non-Targeting siRNA Control Pool (Dharmacon) and siMAX Non Specific siRNA Control 47% GC (AGGUAGUGUAAUCGCCUUG-TT, Eurofins) were used as controls.

### 2.2. Fibroblast Cell Culture and Transfection

For routine culture and morphological experiments, MFF-deficient patient skin fibroblasts and controls (Shamseldin et al. 2012; Koch et al. 2016) were cultured in Dulbecco's Modified Eagle Medium (DMEM), high glucose (4.5 g/L) supplemented with 10% FBS, 100 U/mL penicillin and 100 µg/mL streptomycin at 37°C (5% CO<sub>2</sub> and 95% humidity). The patient cells showed the following mutations in the MFF gene: c.C190T:p.Q64\* (Shamseldin et al. 2012); c.184dup:p.L62Pfs\*13 combined with c.C892T:p.R298\* (Koch et al. 2016; patient 1); c.453\_454del:p.E153Afs\*5 (Koch et al. 2016; patient 2). For assessing peroxisome degradation during starvation, cells were cultured in Hanks' Balanced Salt Solution (HBSS) for the time indicated, and recovered in full DMEM. For assessing peroxisome alterations with microtubule depolymerisation, cells were treated with 10 µM Nocodazole (or 0.07% DMSO as a control), for four hours prior to fixation. MFF-deficient (MFF<sup>Q64\*</sup>) and control human fibroblasts were immortalised by introduction of the SV40 large T antigen. Immortalised fibroblasts (HUFs-T) were cultured in  $\alpha$ -modified Eagle's medium (MEM $\alpha$ ) supplemented with 10% FBS, 2 mM Ultraglutamine 1 (Lonza) and 1 $\times$  MycoZap antibiotics (Lonza) at 37°C (5% CO<sub>2</sub> and 95% humidity). Transfection of fibroblasts was performed using the Neon Transfection System (Thermo Fisher Scientific) as previously described for roGFP2 constructs (Lismont et al. 2017) and siRNA (Schrader and Schrader 2017).

### 2.3. Neuronal Cell Culture and Transfection

Primary hippocampal neuron cultures were prepared from E18 embryonic C57/BL6J mice using a modified protocol of a previously described method (Banker et al. 1998). As standard, pregnant mice [C57BL/6J, delivered at E11 (Janvier Labs, France)] were housed in a 12/12 h light/dark cycle for 1 week, with *ad libitum* access to food and water. Dissected hippocampi were digested by papain enzyme (100 units per ml, Worthington, Biochemical Corp.) for 20 min at 37°C. A homogenous cell suspension was obtained following trituration and filtration, which was then separated from debris by centrifugation [5 min, 180  $\times$  g in BSA solution (7.5%, PAN, BIOTECH)]. Animal protocols were approved by the Ruhr-University Animal Research Board and the State of Baden-Württemberg, Germany. Cells were then seeded into coated 24-well plates (Sarstedt) in Neurobasal medium (Gibco, Life Technologies) supplemented with 1% B27 (Gibco, Life Technologies), 1% horse serum, 1% Glutamax (Gibco, Life Technologies) and penicillin/streptomycin (10,000 units/ml). To maintain the culture, half of the medium was replaced every 2 or 3 times a week by the same medium but containing 2% B27 and without horse serum. For transfection of siRNA and the plasmid encoding EGFP-SKL, the calcium phosphate precipitation method was used at DIV 7 to 9 as described previously (Sun et al. 2013). After 1 hour of incubation at 37 °C, the transfection mixture was washed out of the culture using pre-warmed HBSS (Gibco, Life technologies).

## 2.4. Immunofluorescence and Immunoblotting

Unless otherwise indicated, immunofluorescence was performed 24 hours post-transfection (48 hours for neuronal cells). Cells grown on glass coverslips were fixed for 20 minutes with 4% paraformaldehyde (PFA) in PBS (pH 7.4), permeabilised with 0.2% Triton X-100 for 10 minutes and blocked with 1% BSA for 10 minutes. For neuronal cells, a combined 1 hour permeabilisation and blocking step was used (1% BSA, 0.2% fish skin gelatin, 0.1% Triton X-100). Blocked cells were incubated with primary and secondary antibodies sequentially in a humid chamber for 1 hour. Cells were washed 3 times with PBS between each individual step. Finally, coverslips were washed with ddH<sub>2</sub>O to remove PBS and mounted on glass slides in Mowiol 4-88-containing *n*-propyl gallate as an anti-fading (Bonekamp et al. 2013).

For detection of protein levels, cells were trypsinised, washed in PBS, and centrifuged at 500×*g* for 3 min. Cell pellets were lysed and equal amounts of protein were separated by SDS-PAGE on 12.5% polyacrylamide gels. Transfer to a nitrocellulose membrane (Amersham Bioscience, Arlington Heights, IL, USA) was performed using a semi-dry apparatus (Trans-Blot SD, Bio-rad) and analysed by immunoblotting with enhanced chemiluminescence reagents (Amersham Bioscience, Arlington Heights, IL, USA).

## 2.5. Microscopy

Cell imaging was performed using an Olympus IX81 microscope with an UPlanSApo 100x/1.40 Oil objective (Olympus Optical, Hamburg, Germany). Filters sets eGFP ET (470/40 Et Bandpass filter, Beamsplitter T495 LPXR and 525/50 ET Bandpass filter [Chroma Technology GmbH, Olching, Germany]), and TxRed HC (562/40 BrightLine HC Beamsplitter HC BS 593, 624/40 BrightLine HC [Semrock, Rochester, USA]) were used. Images were taken with a CoolSNAP HQ2 CCD camera.

Live-cell imaging of roGFP2 constructs in HUFs-T fibroblasts was performed with an Olympus IX81 microscope equipped with an UPlanSApo 100x/1.40 Oil objective (Olympus Optical, Hamburg, Germany), BP390-410 and BP470-495 bandpass excitation filters, a dichromatic mirror with a cut-off at 505 nm, a BA510-550 barrier (emission) filter, and a CCD-FV2T digital black and white camera.

Confocal images of MFF<sup>Q64\*</sup> fibroblasts to assess peroxisomal tubule localisation with microtubules were obtained using a Zeiss LSM 880 inverted microscope, with Airyscan spatial detector array (ChA-T1 5.7, ChA-T2 6.9) for super-resolution imaging. The Alpha Plan Apochromat 100×/1.46 oil DIC M27 Elyra objective was used, with lasers 561 nm (15% power) and 488 nm (3% power).

Confocal images of the pHRed probe in fibroblasts were obtained using a Zeiss LSM 510 META inverted microscope equipped with a Plan Apochromat 63×/1.4 NA (oil/dic) objective (Carl Zeiss), using Argon excitation 458 nm and DPSS561 excitation 561 nm, with emission collection 600–620 nm. For detection of peroxisomal pHRed (pHRed-PO) the HC PL APO CS2 63×/1.4 Oil objective was used. For live-cell imaging, cells were plated in 3.5 cm diameter glass bottom dishes (Cellview; Greiner Bio-One). MetaMorph 7 (Molecular Devices, USA) was used to adjust for contrast and brightness.

Confocal images of neuronal cells were collected using a Nikon 90i upright microscope with a Plan Apo 100×/1.45 NA oil objective (Nikon). Laser lines Argon 488 nm and He 543 nm 633nm were used. Imaging parameters include: 1024\*1024 pixels, fixed 0.08µm pixel size, Z-stacks with 4 ~ 7 µm depth and 0.3 µm scanning thickness.

For transmission electron microscopy, fibroblast monolayers were fixed in 0.5% glutaraldehyde in 0.2 M Pipes buffer, pH 7.2, for 15 min at room temperature. Cells were then scraped from the culture dish



and pelleted at 17,000 g for 10 min. Following three buffer washes, the cell pellet was fragmented and postfixed for 1 h in 1% osmium tetroxide (reduced with 1.5% wt/vol potassium ferrocyanide) in 0.1 M sodium cacodylate buffer, pH 7.2. Following three 5 minute washes in distilled water, the pellet fragments were dehydrated through an ethanol gradient and embedded in Durcupan resin (Sigma-Aldrich). 70-nm ultrathin sections were collected on pioloform-coated 100-mesh copper EM grids (Agar Scientific) and contrasted with lead citrate before imaging using a JEOL JEM 1400 transmission electron microscope operated at 120 kV.

## **2.6. Measurement of Peroxisomal Body Size, Tubule Size and Length, and Number**

The Metamorph 7 (Molecular Devices, USA) region measurements function was used for analysis of peroxisome size in MFF-deficient fibroblasts, following calibration of distances for the magnification used. For measurement of peroxisome body and tubule width, transmission EM images were used at 80,000- and 100,000-fold magnification. For measurement of peroxisome length, immunofluorescence images were used at 100-fold magnification and the Metamorph 7 segmented line tool was used. For calculation of peroxisomal number in control fibroblasts, an in-house ImageJ (Schneider et al. 2012) macro was used, utilising the Analyze Particles function. For MFF-deficient patient fibroblasts, peroxisome number was counted manually.

## **2.7. Marker Protein Distribution Measurements**

To measure the fluorescence intensity of PEX14, PMP70, catalase or GFP-SKL over the length of a single peroxisome, cells were first processed for immunofluorescence. After imaging, the Metamorph 7 (Molecular Devices, USA) linescan function was used to assess the distribution of these marker proteins along the peroxisome, with red and green channels overlaid. A 2 pixel width line was drawn along the centre of the peroxisome from the body, along the tubule for a total length of 5  $\mu$ m. The fluorescence intensity for each colour channel was measured with 65 nm increments, and data were normalised to a 0-1 scale, with 1 representing the value of the pixel with the maximum intensity of unsaturated images. Only peroxisomes which did not overlap with other peroxisomes were analysed.

## **2.8. Metabolic and Biochemical Analyses**

Peroxisomal parameters were determined in cultured skin fibroblasts (Ferdinandusse et al. 2016). Concentrations of VLCFAs and C26:0 lysophosphatidylcholine (C26:0 lysoPC) were measured in cultured cells as described previously (Dacremont et al. 1995; Ferdinandusse et al. 2016). Peroxisomal  $\beta$ -oxidation of the VLCFA hexacosanoic acid (C26:0) and pristanic acid were measured as described (Wanders et al. 1995). A D3-C22:0 loading test was performed by loading cells for 3 days with deuterated (D3) C22:0 followed by fatty acid analysis with tandem mass spectrometry, essentially as previously described (Kemp et al. 2004) but with D3-C22:0 instead of D3-C24:0. Peroxisomal phytanic acid  $\alpha$ -oxidation (Wanders and Van Roermund 1993) and the activity of dihydroxyacetone phosphate acyltransferase (DHAPAT), a key enzyme in peroxisomal ether phospholipid synthesis, were measured as described (Ofman and Wanders 1994). Immunoblot analysis was performed with cell homogenates, which were separated by SDS-PAGE and subsequently transferred onto a nitrocellulose membrane using semidry blotting. For visualisation, the secondary antibody IRDye 800 CW goat anti-rabbit was used with the Odyssey Infrared Imaging System (LI-COR Biosciences, Nebraska, USA).

## **2.9. Measurement of Subcellular Redox Dynamics**

The procedures involved in the measurement of subcellular redox levels have been previously described in detail (Lismont et al. 2017). In brief, SV40 large T antigen-transformed human fibroblasts (HUFs-T)

were transfected with plasmids coding for GSH/GSSG- (roGFP2) or H<sub>2</sub>O<sub>2</sub>-sensitive (roGFP2-ORP1) reporter proteins targeted to various subcellular compartments [cytosol (c-), mitochondria (mt-), or peroxisomes (po-)]. One day later, the cells were incubated for 30-60 minutes in phenol red-free culture medium and imaging was performed to visualize both the oxidized (excitation 400 nm, emission 515 nm) and reduced (excitation 480 nm, emission 515 nm) states of roGFP2. During image acquisition, the cells were maintained in a temperature-, humidity-, and CO<sub>2</sub>-controlled incubation chamber. For cytosolic measurements, the ROI was selected outside the nucleus. The Cell<sup>M</sup>/xcellence software module (Olympus) was used to quantify the relative fluorescence intensities of roGFP2 at 400 and 480 nm excitation, giving a ratiometric response.

## 2.10. Measurement of Peroxisomal pH using pHRed

Peroxisomal pH was measured as previously described (Godinho and Schrader 2017). Briefly, MFF-deficient and control fibroblasts were transfected with plasmids coding for a cytosolic or peroxisomal pH-sensitive red fluorescent protein (pHRed-Cyto and pHRed-PO, respectively) (Godinho and Schrader 2017). Twenty four hours after transfection, cells were imaged using excitation wavelengths of 458 and 561 nm. Prior to image acquisition, a controlled temperature chamber was set-up on the microscope stage at 37°C, as well as an objective warmer. During image acquisition, cells were kept at 37°C and in a HEPES-buffered CO<sub>2</sub>-independent medium. For calibration, the cells were incubated in solutions of known pH (containing 5 μM nigericin) in a confocal stage chamber. ImageJ (Schneider et al. 2012) was used to calculate the 561/458 ratiometric response.

## 2.11. Statistical Analysis

A two-tailed, unpaired *t*-test was used to determine statistical differences against the indicated group (\*, *P* < 0.05; \*\*, *P* < 0.01; \*\*\*, *P* < 0.001). Unless indicated otherwise, boxplots are presented with the bottom and top of each box representing the 25th and 75th percentile values, respectively; the horizontal line inside each box representing the median; and the horizontal lines below and above each box denoting the range. Bar graphs are presented as mean ± SEM. In-text data are presented as mean ± SD. Analysis was performed from at least three independent experiments.



266 **Table S1.** Plasmids used in this study

Plasmid	Source
<b>EGFP-SKL</b>	Koch et al. 2005
<b>c-roGFP2</b>	Ivashchenko et al. 2011
<b>mt-roGFP2</b>	Ivashchenko et al. 2011
<b>po-roGFP2</b>	Ivashchenko et al. 2011
<b>c-roGFP2-ORP1</b>	Lismont et al. 2019
<b>mt-roGFP2-ORP1</b>	Lismont et al. 2019
<b>po-roGFP2-ORP1</b>	Lismont et al. 2019
<b>pHRed-Cyto</b>	Godinho and Schrader 2017
<b>pHRed-PO</b>	Godinho and Schrader 2017
<b>HsPEX3(1-44)-EGFP</b>	Fransen et al. 2001

267

268 **Table S2.** Primary and secondary antibodies used in this study

Antibody	Type	Dilution		Source
		IMF	WB	
<b>ACOX1</b>	pc rb	-	1:1000	Proteintech (10957-1-AP) or gift from T. Hashimoto, Japan
<b><math>\alpha</math>-Tubulin</b>	mc ms	-	1:1000	Sigma (T9026)
<b>Catalase</b>	pc ms	1:150	-	Abcam (ab88650)
<b>Catalase</b>	mc ms	-	1:250	Abcam (ab179843)
<b>MAP2</b>	pc gp	1:500	-	Synaptic Systems (188004)
<b>PEX14</b>	pc rb	1:1400	1:4000	D. Crane, Griffith University, Brisbane, Australia
<b>PMP70</b>	pc rb	1:100	-	A. Völkl, University of Heidelberg, Heidelberg, Germany
<b>PMP70</b>	mc ms	1:500	-	Sigma (SAB4200181)
<b>Thiolase</b>	pc rb	-	1:2000	Atlas antibodies (HPA007244)
<b>Alexa Fluor 488</b>	dk anti-rb	1:500	-	ThermoFisher Scientific (A21206)
<b>Alexa Fluor 488</b>	dk anti-ms	1:500	-	ThermoFisher Scientific (A21202)
<b>Alexa Fluor 594</b>	dk anti-rb	1:500	-	ThermoFisher Scientific (A21207)
<b>Alexa Fluor 594</b>	dk anti-ms	1:500	-	ThermoFisher Scientific (A21203)
<b>Alexa Fluor 568</b>	gt anti-gp	1:1000	-	Invitrogen (A-11075)

<b>IRDye 800 CW</b>	gt anti-rb	-	1:12500	Westburg
<b>HRP IgG</b>	gt anti-ms	-	1:10000	Bio-Rad (170-6516)
<b>HRP IgG</b>	gt anti-rb	-	1:10000	Bio-Rad (172-1013)

---

269 Abbreviations: IMF, immunofluorescence; WB, western blot; pc, polyclonal; mc, monoclonal; ms,  
270 mouse; rb, rabbit; gp, guinea pig; gt, goat; dk, donkey; HRP, horseradish peroxidase.

## 3. Results

### 3.1. Morphological characterisation of MFF-deficient peroxisomes

To visualize peroxisomes in different MFF-deficient patient skin fibroblasts (Shamseldin et al. 2012; Koch et al. 2016) under similar conditions, we processed the cells for immunofluorescence microscopy using an antibody against PEX14, a peroxisomal membrane protein. In all three MFF-deficient cell lines, peroxisomes were highly elongated, whereas in controls peroxisomes showed a punctate staining pattern typical for human fibroblasts (**Fig. 1A**). Mitochondria in patient cells were also reported to be elongated (Shamseldin et al. 2012; Koch et al. 2016). In many cells peroxisomes were extremely long ( $> 30 \mu\text{m}$ ); elongation was even more pronounced than in DRP1 patient fibroblasts, which also display tubular peroxisomes and mitochondria (Waterham et al. 2007; Nasca et al. 2016). The elongation of peroxisomes in MFF-deficient fibroblasts has been suggested to be the result of a constant lipid flow from the ER to peroxisomes via membrane contact sites which are mediated by peroxisomal ACBD5 and ER-resident VAPB (Costello et al. 2017b). As peroxisomes cannot divide due to the loss of functional MFF, lipid transfer from the ER results in a pronounced growth/elongation of the peroxisomal membrane. Furthermore, re-introduction of MFF has been shown to restore the normal, punctate peroxisomal phenotype in MFF-deficient fibroblasts (Costello et al. 2017b).

Occasionally, peroxisomes in patient fibroblasts appeared to have a constricted, ‘beads-on-a-string’ phenotype (**Fig. 1A**, Magnifications). Such a phenotype is seen with DRP1 depletion, as peroxisomal constriction can occur independently of DRP1, but fission cannot (Koch et al. 2004). How peroxisomal constriction is mediated is still unclear. A constricted, ‘beads-on-a-string’-like peroxisome morphology in MFF-deficient cells would suggest that peroxisomal constriction can also occur independently of MFF (Ribeiro et al. 2012). However, MFF is also suggested to play a role in the constriction of the peroxisomal membrane, as it localises to peroxisomal constriction sites (Itoyama et al. 2013; Soliman et al. 2018). To confirm constricted peroxisome morphology in MFF-deficient cells, we performed electron microscopy (**Fig. 1B**). In contrast to immunofluorescence, constrictions of elongated peroxisomes were not observed in ultrastructural studies (**Fig. 1B**). Interestingly, EM revealed the presence of spherical peroxisome bodies, with a single, smaller tubule protruding from the body (**Fig. 1B**). We assume that the “constricted” appearance of peroxisomes in immunofluorescence is likely due to instability of the extremely long, delicate membrane structures during fixation with para-formaldehyde, highlighting the importance of ultrastructural studies to validate light microscopy observations. Ultrastructural studies (**Fig. 1B**) and immunofluorescence microscopy (**Fig. 1C**) show that the peroxisomal membrane tubules are frequently aligned along microtubules, which may contribute to tubule stability and maintenance.

Measurement of peroxisomes in EM micrographs revealed that peroxisome bodies are significantly larger than peroxisomal tubules (mean width, body:  $141 \pm 37 \text{ nm}$ , tubule:  $81 \pm 22 \text{ nm}$ ) (**Fig. 1D**). The measured body width is consistent with that of spherical peroxisomes in human fibroblasts from healthy individuals typically being reported to be between 50-200 nm in width (Arias et al. 1985; Galiani et al. 2016). Peroxisome length was also quantified based on immunofluorescence data, with a wide range of lengths being present, from smaller, rod shaped peroxisomes ( $> 3 \mu\text{m}$ ) up to very highly elongated tubules ( $> 30 \mu\text{m}$ ) (mean length,  $8.73 \pm 9.2 \mu\text{m}$ ) (**Fig. 1E**). As expected with a defect in division, the peroxisome number was reduced in MFF-deficient fibroblasts in contrast to controls (mean number, control fibroblasts:  $244 \pm 116$ , dMFF:  $34 \pm 25$ ) (**Fig. 1F**). Overall, we reveal that peroxisomes in MFF-deficient patient fibroblasts are fewer and consist of two continuous membrane domains: a spherical

peroxisome body with typical peroxisome size, and a thin, highly elongated tubular structure protruding from this body.

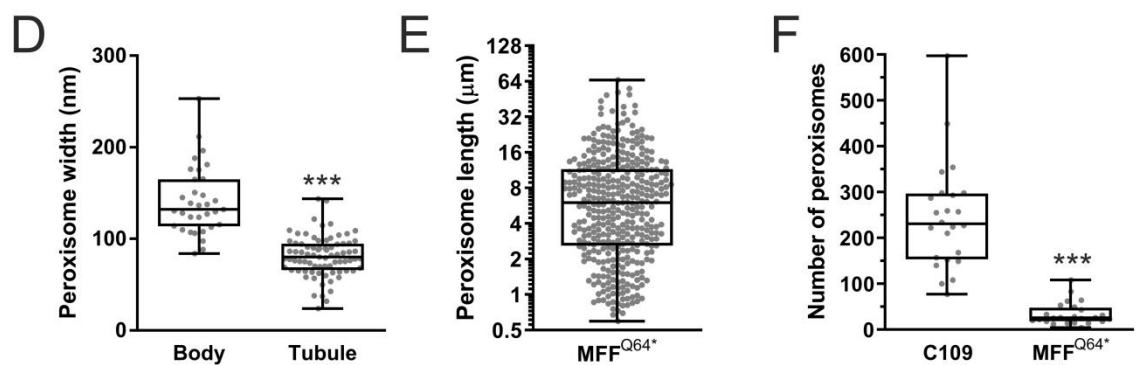
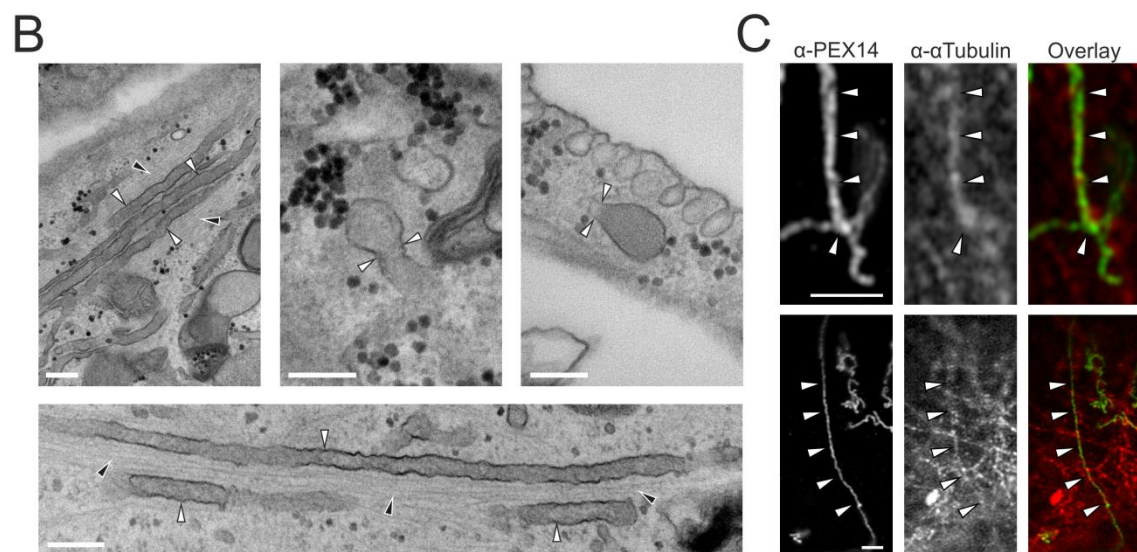
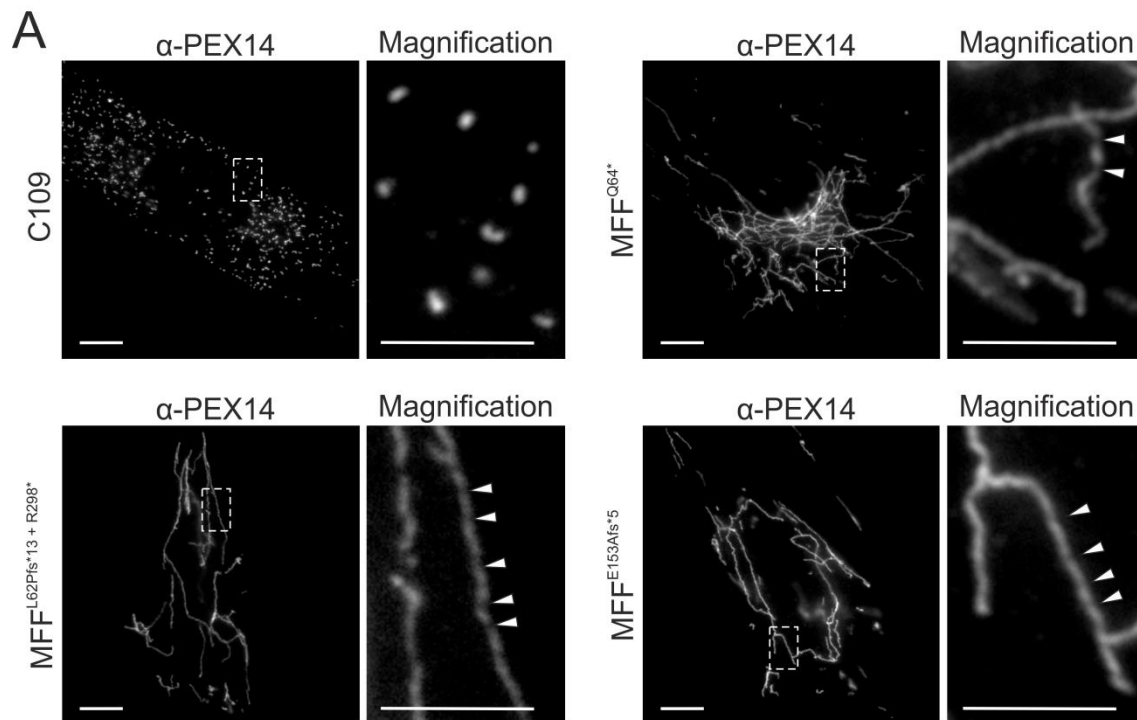


**Figure 1.** Morphological characteristics of peroxisomes in MFF-deficient patient fibroblasts are altered. (A) Control fibroblasts (C109) and MFF-deficient patient fibroblasts [mutations Q64\* (Shamseldin et al. 2012), L62Pfs\*13+R298\* (Koch et al. 2016) and E153Afs\*5 (Koch et al. 2016)] were processed for immunofluorescence microscopy using antibodies directed to PEX14, a peroxisomal membrane marker. Higher magnification of boxed region is shown. Arrowheads highlight potential membrane constrictions. Scale bars, 10  $\mu$ m; magnification, 5  $\mu$ m. (B) Electron micrographs of peroxisomes in MFF-deficient cells (MFF<sup>Q64\*</sup>). White arrowheads highlight peroxisomal membrane tubules, black arrowheads indicate microtubules. Scale bars, 0.2  $\mu$ m. (C) Confocal (Airyscan) images of peroxisomal membrane tubules (anti-PEX14) in MFF<sup>Q64\*</sup> cells co-stained with anti- $\alpha$ -tubulin. White arrowheads indicated co-localisation of peroxisomes and microtubules. Scale bars, 3  $\mu$ m. (D) Measurement of peroxisomal width (nm) of bodies and tubules based on electron micrographs of MFF<sup>Q64\*</sup> fibroblasts [n = 33 (bodies), 79 (tubules)]. (E) Measurement of peroxisomal length ( $\mu$ m) from immunofluorescence images of MFF<sup>Q64\*</sup> patient fibroblasts (n = 392). (F) Quantification of peroxisome number based on immunofluorescence images of control (C109) and MFF<sup>Q64\*</sup> fibroblasts (n = 24). Data are from at least 3 independent experiments. \*\*\*, P < 0.001; two-tailed, unpaired t test.

### 3.2. MFF deficiency does not alter standard biochemical parameters associated with peroxisomal dysfunction

Several biochemical parameters were studied to investigate peroxisomal function in cultured fibroblasts (Table 1). Peroxisomal  $\alpha$ - and  $\beta$ -oxidation activities were measured with different radiolabelled substrates, i.e. [<sup>14</sup>C]-phytanic acid, pristanic acid and cerotic acid (C26:0). In addition, very long-chain fatty acid (VLCFA) metabolism was studied with a three day D3-C22 loading test, and total VLCFA levels and C26-lysophosphatidylcholine levels were determined in cell pellets (Ferdinandusse et al. 2016). No notable abnormalities were found in all three MFF-deficient cell lines providing no indication of a disturbed metabolism of VLCFAs or branched-chain fatty acids in peroxisomes.  $\alpha$ -oxidation values were slightly higher than the reference range, but this does not indicate any dysfunction. The activity of dihydroxyacetone phosphate acyltransferase (DHAPAT), the first enzyme of the plasmalogen biosynthesis pathway located in peroxisomes, was within reference range. The intra-peroxisomal processing of the peroxisomal  $\beta$ -oxidation enzymes acyl-CoA oxidase 1 (ACOX1) and 3-ketoacyl-CoA thiolase was not altered, suggesting normal peroxisomal matrix protein import and processing activity in contrast to fibroblasts from a patient with a peroxisomal biogenesis disorder (Fig. 2). This is in line with metabolic and biochemical analyses of plasma from different MFF patients (Shamseldin et al. 2012; Koch et al. 2016; Nasca et al. 2018). We can confirm from these studies that MFF deficiency does not cause alterations to overall peroxisomal biochemical function. This is also in line with reports from other disorders affecting the dynamics and plasticity of peroxisomes (e.g. DRP1- or PEX11 $\beta$ -deficiency) (Waterham et al. 2007; Ebberink et al. 2012).

	MFF <sup>L62Pfs*13+R298*</sup>	MFF <sup>E153Afs*5</sup>	MFF <sup>Q64*</sup>	Reference range
<b>VLCFAs</b> ( $\mu$ mol/g protein)				
C26:0	0.30	0.33	0.29	0.16-0.41
C26/C22 ratio	0.06	0.07	0.07	0.03-0.1
<b>C26-lysoPC</b> (pmol/mg protein)	12.3	9.2	7.0	2-14
<b>Alpha-oxidation activity</b> (pmol/(hour.mg protein))	135	104	n.d.	28-95
<b>Beta-oxidation activity</b> (pmol/(hour.mg protein))				
C26:0	2109	1505	n.d.	800-2040
Pristanic acid	1072	1099	n.d.	790-1072



<b>D3C22 loading test</b> ( $\mu\text{mol/g protein}$ )				
D3C26 (chain elongation)	0.29	0.3	0.26	0.16-0.66
D3C16/D3C22 ratio ( $\beta$ -oxidation)	1.25	1.74	2.27	0.64-2.13
<b>DHAPAT activity</b> ( $\text{nmol}/(2\text{hour.mg protein})$ )	9.2	7.1	6.6	5.9-15.5

n.d., not determined; VLCFA, very long-chain fatty acid; C26-lysoPC, C26-lysophosphatidylcholine; DHAPAT, dihydroxyacetone phosphate acyltransferase.

**Table 1.** Biochemical parameters associated with peroxisomal dysfunction are normal in MFF-deficient patient fibroblasts. Peroxisomal parameters determined in three MFF-deficient patient fibroblast cell lines MFF<sup>L62Pfs\*13+R298\*</sup> (Koch et al. 2016), MFF<sup>E153Afs\*5</sup> (Koch et al. 2016), and MFF<sup>Q64\*</sup> (Shamseldin et al. 2012). Very long-chain fatty acid (VLCFA) levels, C26-lysophosphatidylcholine (C26-lysoPC),  $\alpha$ - and  $\beta$ -oxidation activity, VLCFA metabolism (D3C22 loading test) and dihydroxyacetone phosphate acyltransferase (DHAPAT) activity were measured. A reference range of control fibroblasts from healthy individuals is shown for comparison.

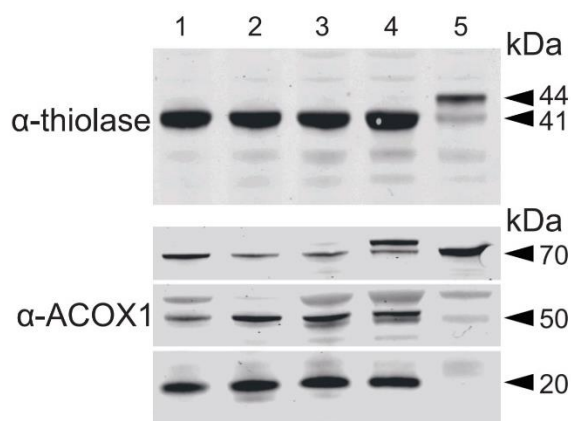


**Figure 2.** Immunoblot analysis of fibroblast homogenates from MFF-deficient patients. Antibodies were directed against peroxisomal 3-ketoacyl-CoA thiolase (upper panel) or peroxisomal acyl-CoA oxidase 1 (ACOX1; lower panel). Lanes 1-3, MFF-deficient patient fibroblasts MFF<sup>Q64\*</sup> (Shamseldin et al. 2012), MFF<sup>L62Pfs\*13+R298\*</sup> (Koch et al. 2016) and MFF<sup>E153Afs\*5</sup> (Koch et al. 2016), respectively. Lane 4: control subject, Lane 5: fibroblasts of a patient with Zellweger Spectrum Disorder (ZSD). Results show normal proteolytic processing of 3-ketoacyl-CoA thiolase (40-kDa) and ACOX1 (50- and 20-kDa) in the MFF-deficient cell lines, whereas in the ZSD line the unprocessed bands of 3-ketoacyl-CoA thiolase (44-kDa) and ACOX1 (70-kDa) are present. Note that the protein band above the 70 kDa band of ACOX1 is non-specific.

### 3.3. Protein import into MFF-deficient peroxisomes is impaired in the tubular extensions

As globular peroxisomal bodies were visible in ultrastructural studies (**Fig. 1B**) but surprisingly less visible in immunofluorescence studies with anti-PEX14, which labelled predominantly tubular structures (**Fig. 1A**), we performed co-localisation studies with anti-catalase, a prominent peroxisomal marker enzyme in the peroxisomal matrix (**Fig. 3A**). In contrast to PEX14, endogenous catalase was found to localise primarily to the spherical peroxisome bodies, with weaker fluorescence intensity along the peroxisomal tubules (**Fig. 3A**). Analysis of fluorescence intensity along single peroxisomes of both PEX14 and catalase confirmed PEX14 fluorescence primarily along tubules with some localisation in bodies, whereas catalase fluorescence was primarily detected in the peroxisomal body, with reduced



intensity along the tubule (**Fig. 3A**). Peroxisomes import matrix proteins from the cytosol via dedicated import machinery at the peroxisomal membrane (Francisco et al. 2017). Matrix proteins such as catalase are imported into peroxisomes via a C-terminal peroxisomal targeting signal (PTS1). These steady-state observations imply that catalase is mainly imported into the spherical bodies, suggesting that those represent mature, import-competent structures. To test this hypothesis, we expressed a GFP-fusion protein with a C-terminal PTS1 signal SKL (GFP-SKL) in MFF-deficient cells. Cells were processed for immunofluorescence after 24 hours and labelled with anti-PEX14 antibodies (**Fig. 3B**). Similar to endogenous catalase, exogenously expressed GFP-SKL localised primarily to peroxisomal bodies, with less presence in the peroxisomal tubules (**Fig. 3B**). This was confirmed by analysis of fluorescence intensity (**Fig. 3B**). Immunofluorescence microscopy with the peroxisomal membrane markers PMP70 and PEX14 revealed co-localisation of both membrane proteins at membrane tubules (**Fig. 3C**). PMP70 also localised to the spherical bodies, where PEX14 is less prominent (**Fig. 3C**). These findings indicate that the spherical bodies represent mature, import-competent peroxisomes, whereas the tubular extensions comprise a pre-peroxisomal membrane compartment which either has not yet fully acquired import competence for matrix proteins or lacks the capability to retain them.

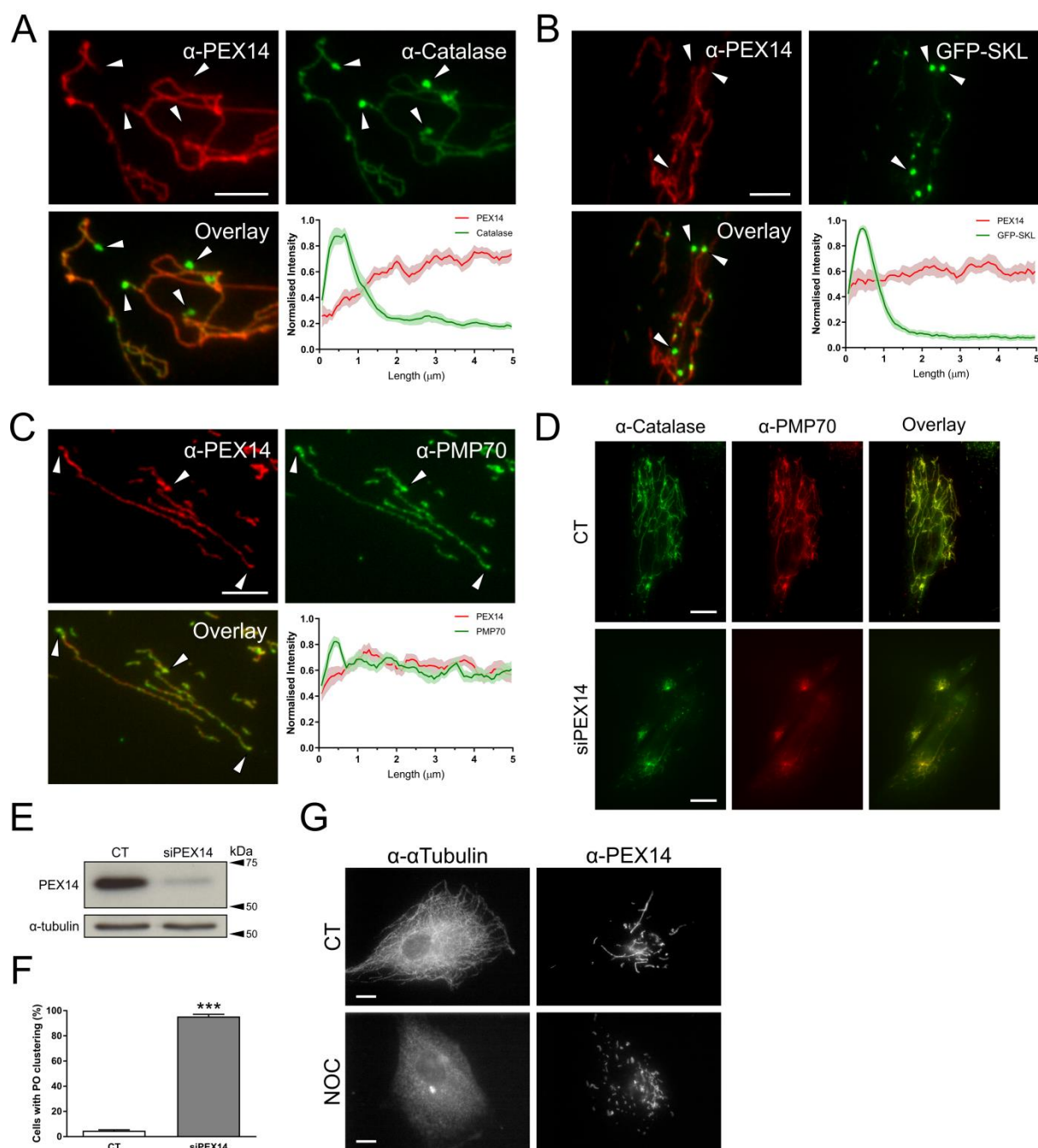


**Figure 3.** Altered marker protein distribution in MFF-deficient patient fibroblasts (MFF<sup>Q64\*</sup>). Patient fibroblasts were processed for immunofluorescence microscopy using antibodies against peroxisomal membrane markers PEX14 and PMP70 (A) or PEX14 and catalase (B), and fluorescence intensity measured along 5  $\mu$ m of peroxisome, starting at peroxisome bodies (arrowheads) normalised to the maximum intensity. Shaded area in graphs represents the standard error of the mean (line) (n = 12). Arrowheads highlight peroxisomal bodies. Scale bar, 5  $\mu$ m. (C) Patient fibroblasts were transfected with a plasmid encoding EGFP-SKL and processed for immunofluorescence microscopy using an antibody against PEX14. Quantification was performed as in A, B (n = 12). Arrowheads highlight peroxisomal bodies. Scale bar, 5  $\mu$ m. (D) MFF<sup>Q64\*</sup> fibroblasts were transfected with control (CT) or PEX14 siRNA (siPEX14), and processed for immunofluorescence microscopy after 48 hours using antibodies against catalase and PMP70. Scale bars, 10  $\mu$ m. (E) Immunoblotting of control (CT) or PEX14 siRNA (siPEX14) transfected patient fibroblasts, using antibodies against PEX14 and  $\alpha$ -tubulin

(loading control). **(F)** Quantification of peroxisomal clustering in MFF-deficient fibroblasts either transfected with control (CT) or PEX14 siRNA (siPEX14) (n = 150). Data are from at least 3 independent experiments. \*\*\*,  $P < 0.001$ ; two-tailed, unpaired t test. **(G)** MFF<sup>Q64\*</sup> patient fibroblasts were treated with 0.07% DMSO (CT), or 10  $\mu$ M nocodazole (NOC) for four hours prior to processing for immunofluorescence microscopy using antibodies against  $\alpha$ -tubulin and PEX14. Scale bars, 10  $\mu$ m.

### 3.4. A role of PEX14 in maintaining peroxisomal tubule stability

As PEX14 is part of the matrix protein import machinery (Brown and Baker 2008), its predominant localisation to the peroxisomal membrane tubules (rather than the import-competent spherical bodies) is unexpected. However, additional functions for PEX14 have been suggested. Peroxisomes interact with and move along microtubules (Thiemann et al. 2000; Schrader et al. 2003; Castro et al. 2018). The N-terminal domain of PEX14 (1-78) has previously been shown to bind tubulin (Bharti et al. 2011; Theiss et al. 2012). Although PEX14 is not essential for microtubule-dependent peroxisomal motility (Castro et al. 2018), it may function as a peroxisomal microtubule docking factor. Indeed, in ultrastructural and confocal studies microtubules were frequently observed in close association with the entire length of peroxisomal tubules in MFF patient cells (**Fig. 1B, C**). Furthermore, in a previous study, we showed that highly elongated peroxisomal tubules in fibroblasts are associated with microtubules, and that tubule elongation is reduced in PEX14-deficient cells (Castro et al. 2018). Based on these observations, we hypothesised that PEX14 may be required for the stabilisation of highly elongated peroxisomal tubules. To test this, we depleted PEX14 by siRNA-mediated knock down in MFF-deficient cells (**Fig. 3D-F**). Peroxisomal tubules in these cells are typically stretched out in the cell, allowing for easy visualisation. However, when PEX14 was knocked down, peroxisomes lost their tubular morphology and appeared clustered or fragmented (**Fig. 3D**) (cells with clustered/fragmented morphology: control siRNA:  $4.7 \pm 1.2\%$ , PEX14 siRNA:  $95.3 \pm 3.1\%$ ) (**Fig. 3F**). The peculiar peroxisome morphology was specific for silencing of PEX14, and was not observed after silencing of PEX11 $\beta$  or ACBD5 in MFF-deficient cells (Costello et al. 2017b). Clustering and fragmentation of elongated peroxisomes in MFF-deficient cells was also observed after depolymerisation of microtubules with nocodazole (**Fig. 3G**). These observations suggest a role for PEX14 in facilitating and stabilising peroxisomal membrane extensions by linking the peroxisomal membrane to microtubules. This may explain why PEX14 is predominantly localising to the highly elongated peroxisomal membranes in MFF patient cells.

### 3.5. Peroxisomal redox state and pH levels are altered in MFF-deficient fibroblasts

The metabolic parameters of peroxisomes in MFF-deficient cells were normal, in particular their different functions in lipid metabolism (**Table 1**). As peroxisomes play a role in cellular H<sub>2</sub>O<sub>2</sub> metabolism and redox homeostasis, we also investigated these parameters (**Fig. 4**). Firstly, we assessed the glutathione disulphide (GSSG) to glutathione (GSH) ratio, a marker of oxidative balance. Therefore, MFF-deficient SV40 large T antigen-transformed human fibroblasts (HUFs-T) were transfected with a plasmid encoding cytosolic, mitochondrial or peroxisome-targeted roGFP2 (**Fig. 4A**). RoGFP2 is a highly responsive, pH-independent sensor for the glutathione redox couple, and oxidation causes a shift of its excitation maximum from 488 nm to 405 nm (Ivashchenko et al. 2011; Lismont et al. 2017). Analyses of the 400/480 ratiometric responses of peroxisome-targeted roGFP2 revealed that the intra-peroxisomal pool of glutathione is less oxidized in the MFF-deficient fibroblasts than in the control cells (**Fig. 4B**). In contrast, no alterations in the glutathione redox state could be detected in the cytosol or the mitochondrial matrix.

To monitor changes in hydrogen peroxide homeostasis, MFF-deficient HUFs-T and controls were transfected with plasmids coding for cytosolic, mitochondrial, or peroxisome-targeted roGFP2-ORP1, a H<sub>2</sub>O<sub>2</sub>-responsive variant of roGFP2 (**Fig. 4C**) (Lismont et al. 2019b). No changes in oxidation state were observed in the cytosol and mitochondria (**Fig. 4D**). However, for peroxisomes, a decreased 400/480 nm ratiometric response was seen (**Fig. 4D**), indicating reduced levels of H<sub>2</sub>O<sub>2</sub> inside peroxisomes in MFF-deficient cells.

In addition, we used peroxisome-targeted pHRed (pHRed-PO), another ratiometric probe, to assess peroxisomal pH in MFF-deficient patient fibroblasts (Tantama et al. 2011; Godinho and Schrader 2017). Importantly, this sensor is insensitive to changes in H<sub>2</sub>O<sub>2</sub> levels (Tantama et al. 2011). The pHRed-PO probe successfully targets to peroxisomes in control and MFF-deficient fibroblasts (**Fig. 4E**). It mainly distributes to the import-competent spherical peroxisomal bodies, but also to the membrane tubules (**Fig. 4E**). Following calibration of the pHRed probe (**Fig. 4F**), the intra-peroxisomal pH can be calculated based on the 458/561 nm ratiometric response. Interestingly, intra-peroxisomal pH in MFF-deficient fibroblasts was found to be more alkaline than in control fibroblasts (**Fig. 4G**) (mean peroxisomal pH, control:  $7.24 \pm 0.30$ , patient fibroblasts:  $8.00 \pm 0.29$ ).

Overall, these findings point towards alterations in the peroxisomal redox environment. Specifically, we observed a decrease in the GSSG/GSH ratio and H<sub>2</sub>O<sub>2</sub> levels in MFF-deficient fibroblasts. In addition, we have shown that absence of MFF results in a more alkaline intra-peroxisomal pH. This suggests that MFF-deficiency may compromise normal peroxisomal redox regulation.

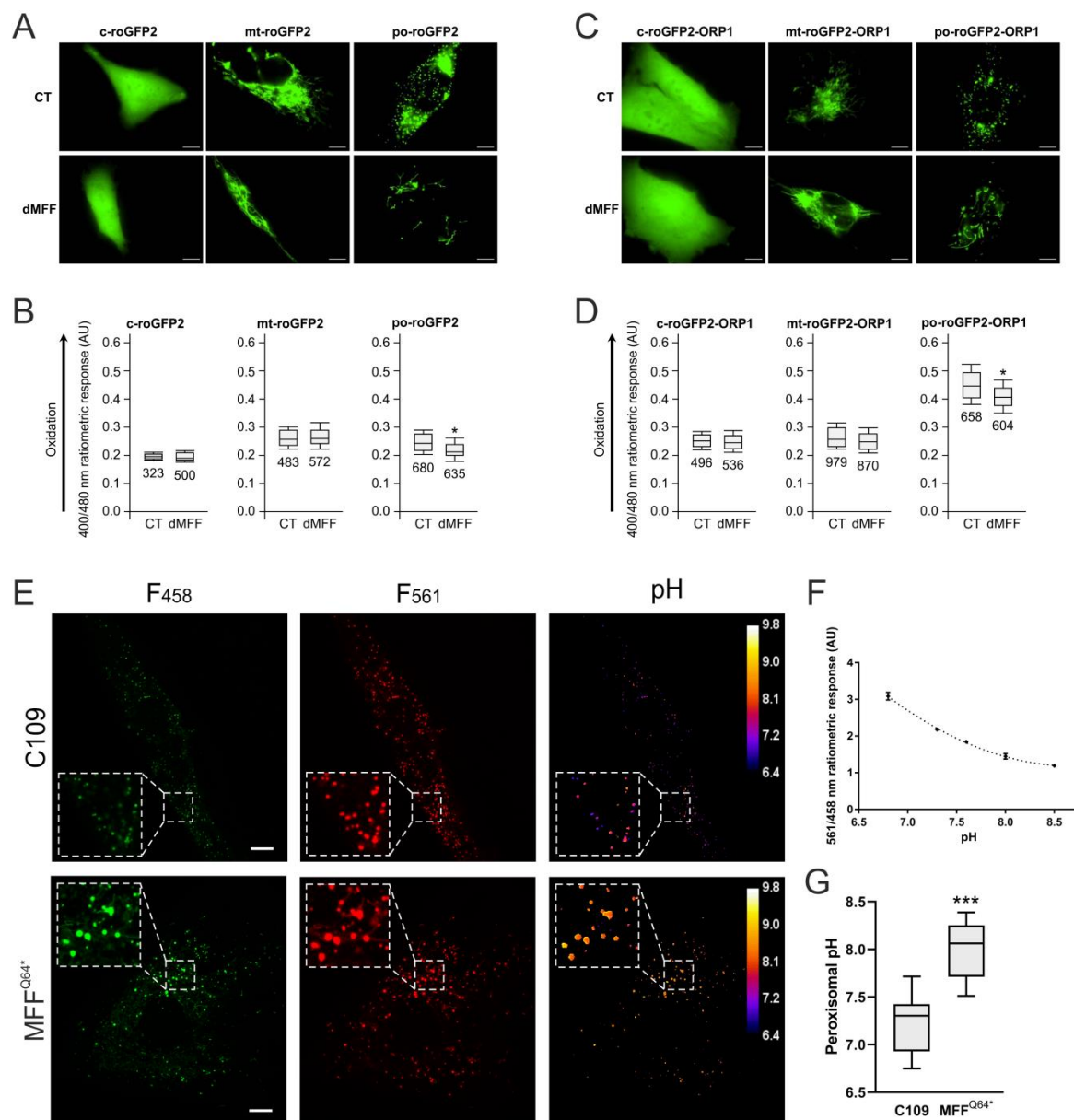


**Figure 4.** Peroxisomal redox state and pH levels are altered in MFF-deficient fibroblasts. Control (CT) or MFF-deficient (dMFF) SV40 large T antigen-transformed human fibroblasts (HUFs-T) were transfected with a plasmid encoding cytosolic (c-), mitochondrial (mt-) or peroxisomal (po-) roGFP2 (A, B) or roGFP2-ORP1 (C, D). (A) Distribution patterns of the respective roGFP2 proteins. (B) Box plot representations of the 400/480 nm fluorescence response ratios of the respective roGFP2 proteins. (C) Distribution patterns of the respective roGFP2-ORP1 proteins. (D) Box plot representations of the 400/480 nm fluorescence response ratios of the respective roGFP2 proteins. The bottom and top of each box represent the 25th and 75th percentile values, respectively; the horizontal line inside each box represents the median; and the horizontal lines below and above each box denote the mean minus and plus one standard deviation, respectively. The total number of measurements (two independent experiments; minimum 15 individual measurements in at least 20 randomly chosen cells) is indicated below each box plot. The data from the dMFF cell line were statistically compared with those from the CT cell line (\*\*,  $p < 0.01$ ). (E) Distribution patterns of pHRed-PO in control (C109) and MFF-deficient patient fibroblasts (MFF<sup>Q64\*</sup>) at excitation wavelengths of 458 and 561 nm, along with digital visualisation of individual peroxisomal pH levels. Higher magnification views of boxed regions are indicated. (F) Calibration of the pHRed probe using cytosolic pHRed. The 458/561 ratiometric response

is given at each pH level. AU, arbitrary units. **(G)** Quantification of peroxisomal pH in control (C109) and MFF<sup>Q64\*</sup> cells, converting the ratiometric response to pH using the calibration curve (n=20). Scale bars, 10  $\mu$ m. Data are from at least 2-3 independent experiments. \*, P < 0.05; \*\*\*, P < 0.001; two-tailed, unpaired t test.

### 3.6. MFF knockdown in neuronal cells increases peroxisomal clustering

Peroxisomal disorders are typically associated with neurological alterations (Berger et al. 2016), including disorders with a deficiency in peroxisomal dynamics and plasticity such as PEX11 $\beta$ , DRP1 and MFF (Waterham et al. 2007; Shamseldin et al. 2012; Ebberink et al. 2012; Koch et al. 2016; Sheffer et al. 2016; Nascia et al. 2018). To investigate potential morphological alterations of peroxisomes after depletion of MFF in neuronal cells, primary mouse hippocampal neurons were transfected with a plasmid encoding EGFP-SKL and MFF-specific or control siRNA. After 48 hours, cells were processed for immunofluorescence using anti-MAP2 as a neuronal dendrite marker (**Fig. 5**). With control siRNA, peroxisomes in neuronal cells were typically punctate, with an even distribution in the soma (**Fig. 5, CT**). In contrast, peroxisomes in MFF-depleted cells appeared clustered and enlarged with a brighter fluorescence, losing the even distribution throughout the cell (**Fig. 5, siMFF**) (approx. 77% of MFF-siRNA-treated cells showed this altered phenotype). In contrast to loss of MFF in fibroblasts, peroxisomes in neuronal cells did not hyper-elongate, but form smaller, rod-shaped structures in addition to peroxisomal aggregates. It is possible that an altered peroxisomal phenotype in neurons may contribute to the neurological abnormalities observed in MFF-deficiency.



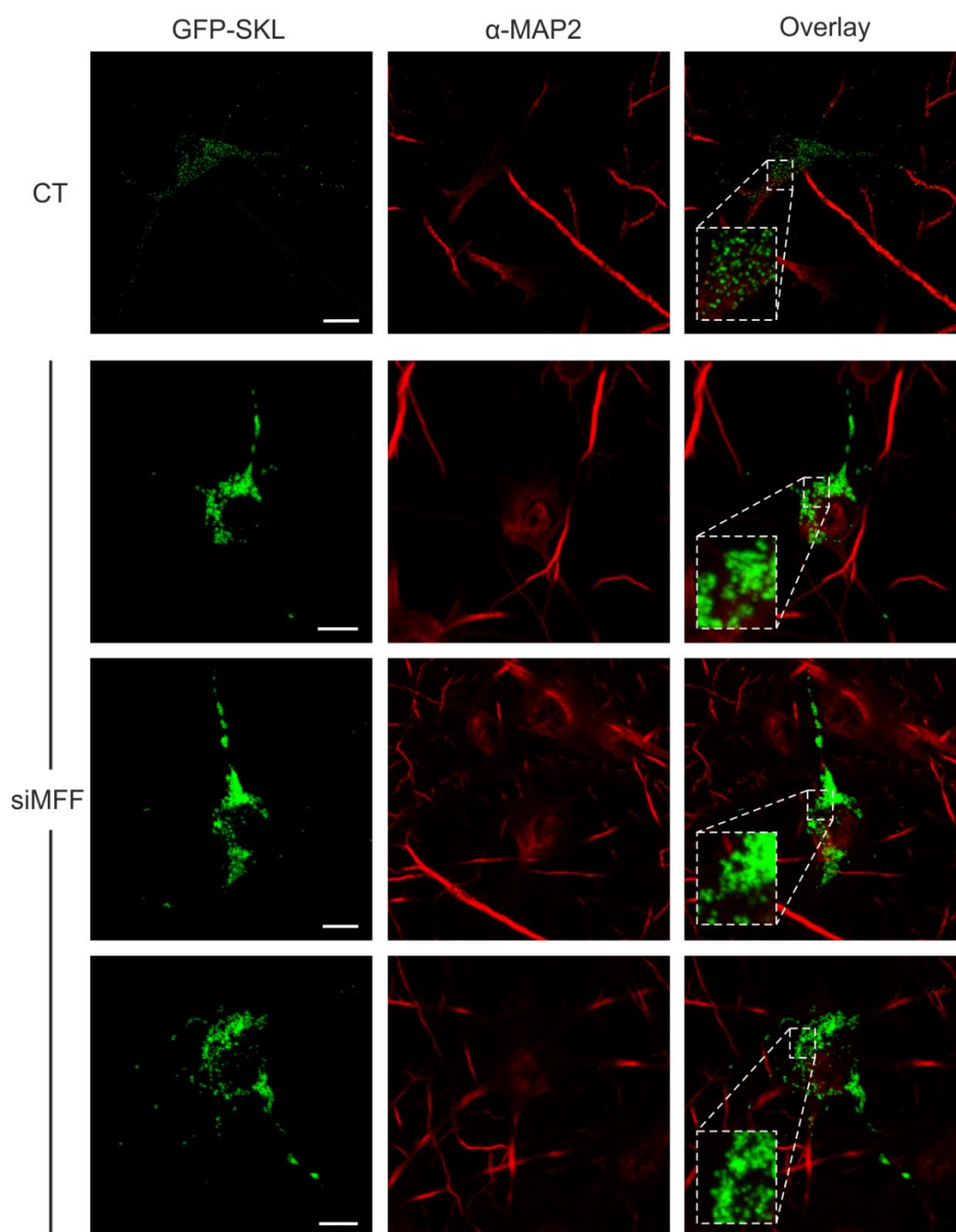


**Figure 5.** Alterations to peroxisomal morphology in MFF-depleted neuronal cells. (A) Primary mouse hippocampal neurons were transfected with plasmids encoding EGFP-SKL and MFF-specific (siMFF) or control (CT) siRNAs. After 48 hours, cells were processed for immunofluorescence using anti-MAP2 as a neuronal dendrite marker. Representative images are shown. Note that peroxisomes in MFF-depleted cells appear clustered and enlarged with a brighter fluorescence, losing their uniform distribution when compared to controls (see inset images). All images (CT, siMFF) were captured with the same exposure time. Scale bars, 10  $\mu$ m.

### 3.7. Highly elongated peroxisomes in MFF-deficient fibroblasts can be degraded by autophagic processes

Autophagic processes are important for the maintenance of cellular homeostasis and the integrity of organelles (Anding and Baehrecke 2017). Peroxisome homeostasis is achieved via a tightly regulated interplay between peroxisome biogenesis and degradation via selective autophagy (pexophagy) (Eberhart and Kovacs 2018). It is still debated if highly elongated peroxisomes are spared from pexophagy, e.g. due to physical limitations, as the elongated peroxisomes may not fit into the autophagosome. Such a scenario would prevent degradation of peroxisomes and could have pathophysiological consequences.

To examine if highly elongated peroxisomes in MFF-deficient fibroblasts can be degraded by autophagic processes, we first induced pexophagy by the expression of a fragment of peroxisomal biogenesis protein PEX3. Expression of the first 44 amino acids of the peroxin PEX3, which can insert into the peroxisome membrane, was observed to cause complete removal of peroxisomes (Soukupova et al. 1999). When expressing *HsPEX3*(1-44)-EGFP in control fibroblasts (**Fig. 6A, B**), peroxisomes were greatly reduced in number, with many GFP expressing cells showing almost complete loss of PEX14 labelling (**Fig. 6A, CON**). As reported earlier, loss of peroxisomes resulted in mistargeting of *HsPEX3*(1-44)-EGFP to the mitochondria (Soukupova et al. 1999). Interestingly, in MFF-deficient fibroblasts, expression of *HsPEX3*(1-44)-EGFP also caused a marked reduction of peroxisomes (**Fig. 6A, middle panel, B**) or complete loss of PEX14 labelling (**Fig. 6A, lower panel, B**). Increased mitochondrial mistargeting of *HsPEX3*(1-44)-EGFP was observed with increased loss of peroxisomes (**Fig. 6A**).

To examine peroxisome degradation under more physiological conditions, we applied nutrient deprivation. Limiting amino acids in the growth media of cells has been previously shown to induce removal of peroxisomes (Sargent et al. 2016). For assessing peroxisome degradation, controls and MFF-deficient fibroblasts were cultured in Hanks' Balanced Salt Solution (HBSS), which lacks amino acids. After 0, 24 and 48 hours, cells were processed for immunofluorescence using anti-PEX14 as a peroxisomal marker (**Fig. 6C**). In control cells, we observed a marked decrease in spherical peroxisomes, with often only a few organelles remaining after 48 hours in HBSS (**Fig. 6C, D**). As with *HsPEX3*(1-44)-EGFP, we also observed a decrease in peroxisomes in nutrient-deprived MFF-deficient cells, which was accompanied by a significant reduction in peroxisomal length (mean peroxisomal length, 0 hours HBSS:  $6.08 \pm 4.90 \mu\text{m}$ , 48 hours HBSS:  $1.55 \pm 1.43 \mu\text{m}$ ) (**Fig. 6C, E**). The reduction in peroxisomes was accompanied by a reduction in peroxisomal marker proteins (**Fig. 6F**). Peroxisomes and protein levels recovered in control and MFF-deficient cells after switching to complete culture medium for 24 hours (**Fig. 6C-F**). Interestingly, the switch to complete growth medium resulted in the recovery of elongated peroxisomes (mean peroxisomal length, 24 hours recovery:  $3.84 \pm 3.40 \mu\text{m}$ ) (**Fig. 6E**), indicating that peroxisomes in MFF-deficient fibroblasts are still dynamic under certain conditions. Overall, these data show that highly elongated peroxisomes in MFF-deficient cells are not spared from autophagic processes and can be degraded similar to controls. It is thus unlikely that impaired peroxisome degradation contributes to the pathology of MFF-deficiency.

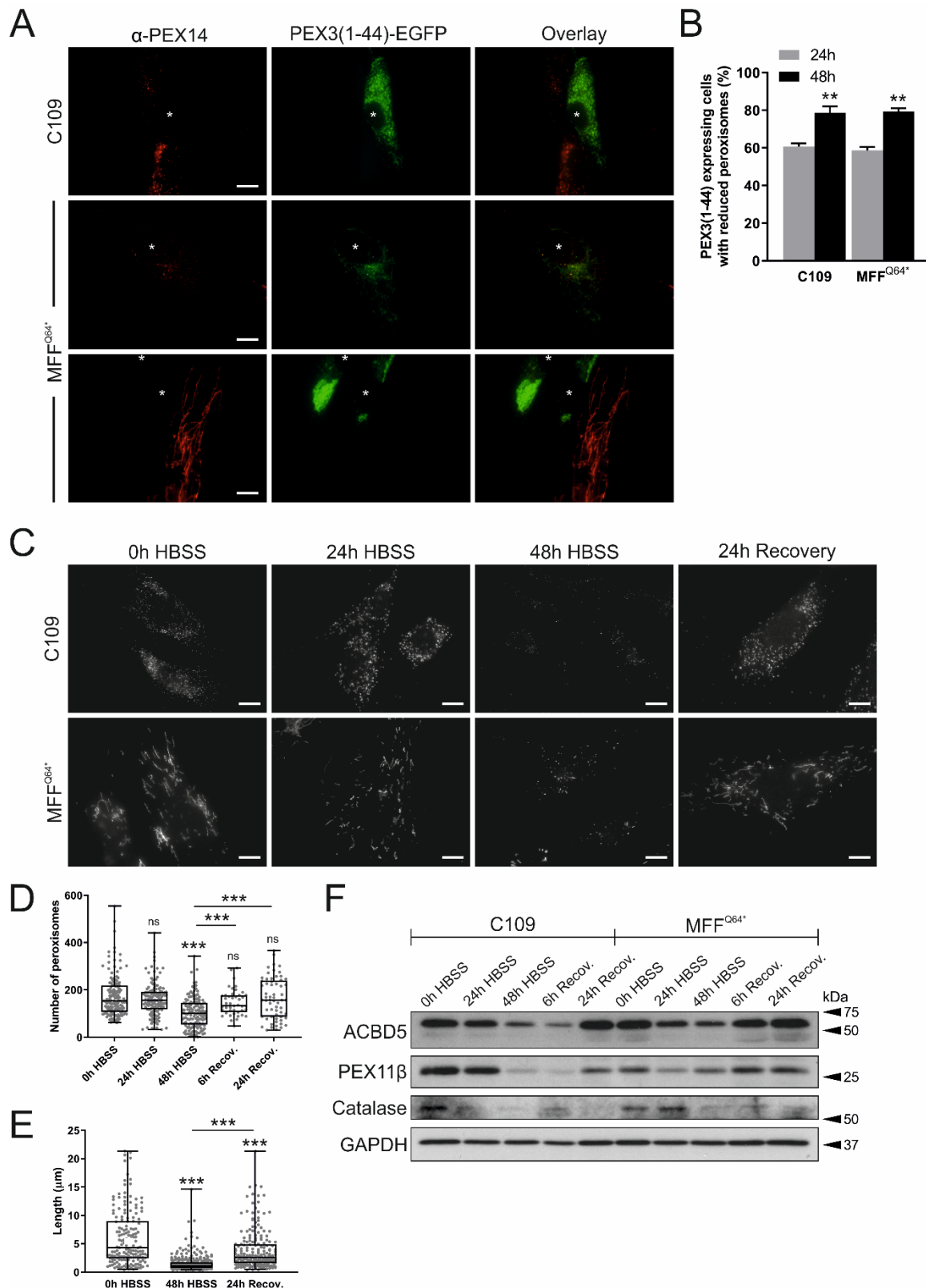


**Figure 6.** Degradation of peroxisomes in MFF-deficient patient fibroblasts. (A) Human control (C109) or MFF-deficient (MFF<sup>Q64\*</sup>) fibroblasts were transfected with a plasmid coding for *Hs*PEX3(1-44)-EGFP to induce peroxisome degradation and processed for immunofluorescence after 24 and 48 hours using antibodies against PEX14. Note the almost complete loss of PEX14, and mistargeting of *Hs*PEX3(1-44)-EGFP to mitochondria when peroxisomes are lost (Soukupova et al. 1999). Asterisks

indicate HsPEX3(1-44)-EGFP expressing cells. Scale bars, 10  $\mu$ m. **(B)** Quantification of HsPEX3(1-44)-EGFP expressing cells (control fibroblasts, CON; MFF-deficient, MFF<sup>Q64\*</sup>) showing reduced peroxisomes after 24 and 48 hours (n = 150). **(C)** Human control (C109) and MFF-deficient fibroblasts (MFF<sup>Q64\*</sup>) were incubated in Hanks' Balanced Salt Solution (HBSS) to induce peroxisome degradation and processed for immunofluorescence after 0, 24 and 48 hours and after 24 hours recovery in complete culture medium using antibodies against PEX14. Scale bars, 10  $\mu$ m. **(D)** Immunoblot of cell lysates from control (C109) and MFF-deficient fibroblasts (MFF<sup>Q64\*</sup>) which were incubated in HBSS for 0, 24, and 48 hours, and after 6 and 24 hours of recovery in complete culture medium. Antibodies against the peroxisomal membrane proteins ACBD5, PEX11 $\beta$  and Catalase were applied. Anti-GAPDH was used as a loading control. Equal amounts of protein were loaded. Molecular mass markers (kDa) are indicated on the right. **(E)** Quantification of the number of peroxisomes in C109 control fibroblasts following incubation in HBSS and recovery in complete culture medium (see **C**) [n = 62 (24h Recovery) to 139 (48h HBSS)]. **(F)** Quantification of peroxisome length in MFF<sup>Q64\*</sup> fibroblasts following 0, 48 hours of HBSS treatment, and after 24 hours of recovery in complete culture medium [n = 167 (0h HBSS) to 297 (48h HBSS)]. Data are from at least 3 independent experiments. \*\*\*, P < 0.001; ns, not significant; two-tailed, unpaired t test.

## 4. Discussion

Whereas dysfunctional peroxisome metabolism and associated diseases are generally well studied, the consequences and pathophysiology caused by specific disruption to peroxisome dynamics and plasticity are less clear. Mutations in *DRP1*, *MFF* or *PEX11 $\beta$*  have been linked to defects in the membrane dynamics and division of peroxisomes rather than to loss of metabolic functions (Waterham et al. 2007; Shamseldin et al. 2012; Ebberink et al. 2012; Koch et al. 2016; Taylor et al. 2017; Nasca et al. 2018). This is in contrast to the classical peroxisome biogenesis disorders (e.g. Zellweger spectrum disorders) or single enzyme deficiencies and can complicate diagnosis through metabolic biomarkers. Despite considerable progress in the field, the precise molecular functions of several of the proteins regulating peroxisomal plasticity remain to be determined as well as the contribution of impaired peroxisomal dynamics to the pathophysiology of the above disorders. In line with this, depletion of *PEX11 $\beta$*  in epidermal cells was recently reported to result in abnormal mitosis and organelle inheritance, thus affecting cell fate decisions (Asare et al. 2017). As *DRP1* and *MFF* also localise to mitochondria, and as loss of *DRP1* or *MFF* function also inhibits mitochondrial division, focus has so far mainly been on mitochondrial properties under those conditions. Here, we assessed the extent to which peroxisomal functions and properties are altered in *MFF*-deficient cells.

There are currently six patients with *MFF*-deficiency identified, with various mutations in the *MFF* protein shown; c.C190T:p.Q64\* (Shamseldin et al. 2012); c.184dup:p.L62Pfs\*13 combined with c.C892T:p.R298\* (Koch et al. 2016); c.453\_454del:p.E153Afs\*5 (Koch et al. 2016); and most recently c.C892T:p.R298\* alone (Nasca et al. 2018). Patient skin fibroblasts show a loss of *MFF* function with mitochondrial and peroxisomal hyper-elongation, and the patients themselves present with neurological abnormalities, showing developmental delay, peripheral neuropathy, optic atrophy, and Leigh-like encephalopathy (Shamseldin et al. 2012; Koch et al. 2016; Nasca et al. 2018). We confirmed a similar degree of peroxisomal hyper-elongation in skin fibroblasts from three different patients suffering from *MFF*-deficiency when maintained under the same culture conditions. Furthermore, peroxisomal biochemical parameters related to fatty acid  $\alpha$ - and  $\beta$ -oxidation, plasmalogen biosynthesis, or matrix protein import/processing did not reveal any deficiencies in fibroblasts from those patients. This is in agreement with biochemical studies in other *MFF*-deficient patient fibroblasts (Koch et al. 2016; Nasca et al. 2018). Overall, these findings support the notion that defects in the membrane dynamics and division of peroxisomes rather than loss of metabolic functions contribute to the disease pathophysiology.

Similar observations in *PEX11 $\beta$* - or *DRP1*-deficient cells (Waterham et al. 2007; Ebberink et al. 2012) have led to the general assumption that defects in peroxisomal dynamics and division result in elongated peroxisomes, which are, however, largely functional and otherwise normal. We now reveal in *MFF*-deficient cells that this is not the case. We show that the elongated peroxisomes in those cells are composed of a spherical body, which represents a mature, import-competent peroxisome, and of thin, tubular extensions, which likely represent pre-peroxisomal membrane compartments; not yet fully import-competent for peroxisomal matrix proteins. An alternative interpretation may be that the tubular structures are to some degree import-competent but lack mechanisms to retain the imported matrix proteins. Such a mechanism for retaining matrix proteins may be provided by membrane constriction, which is impaired in *MFF*-deficient cells.

These observations are consistent with the proposed multi-step maturation model of peroxisomal growth and division and with previous data on tubular membrane extensions after expression of *PEX11 $\beta$*  (Delille et al. 2010; Schrader et al. 2012, 2016). In this respect, elongated peroxisomes in *MFF*-deficient cells resemble those observed after expression of a division-incompetent *PEX11 $\beta$* , which also



results in elongated peroxisomes with an import-competent spherical body and a pre-peroxisomal membrane expansion (Delille et al. 2010). In contrast, elongated peroxisomes in DRP1-depleted cells are constricted, with a “beads-on-a string” like appearance, and the interconnected spherical peroxisomes (“beads”) are import-competent for matrix proteins (Koch et al. 2004). These constrictions may therefore provide a mechanism to retain matrix proteins. This indicates that a defect in MFF influences peroxisome division earlier than a defect in DRP1, and results in a maturation defect of elongated peroxisomes, which are unable to constrict and to subsequently import and/or retain matrix proteins. In line with this, it has recently been shown that MFF can act as a sensor but also potentially as an inducer of mitochondrial constriction (Helle et al. 2017). We propose that MFF deficiency, which impairs peroxisomal membrane constriction and proper assembly of the division machinery, blocks further maturation of the pre-peroxisomal membrane compartment.

This means that, although the number of fully functional peroxisomes is reduced and matrix proteins are largely restricted to the mature spherical bodies, membrane surface area and volume of the peroxisomal compartment are increased in MFF-deficient cells (mean estimated total surface area, control fibroblasts:  $1.55 \times 10^7 \pm 7.29 \times 10^6 \text{ nm}^2$ , dMFF:  $1.15 \times 10^8 \pm 6.57 \times 10^8 \text{ nm}^2$ ; mean estimated total volume, control fibroblasts:  $4.1 \times 10^8 \pm 1.94 \times 10^8 \text{ nm}^3$ , dMFF  $2.5 \times 10^9 \pm 1.45 \times 10^9 \text{ nm}^3$ ) (**Suppl. Fig. S1**), as well as the surface area to volume ratio (mean estimated SA:V, control fibroblasts:  $0.038 \pm 0.001$ , dMFF:  $0.046 \pm 0.005$ ) (**Suppl. Fig. S1**). This likely explains why biochemical functions of elongated peroxisomes are overall normal under standard conditions. However, it can be speculated that sudden environmental changes (e.g. an increase in peroxisomal substrates via nutrients/diet or stress conditions), which require increased peroxisomal metabolic activity and number, will overwhelm the capacity of the peroxisomal compartment in MFF-deficient cells. This may also explain why mild alterations of peroxisomal metabolism are occasionally observed in patients with defects in peroxisomal dynamics and division (Waterham et al. 2007; Ebberink et al. 2012; Taylor et al. 2017). Furthermore, peroxisomes in patient cells may be less able to cope with increased expression of peroxisomal matrix enzymes or PMPs. Those may accumulate in the cytoplasm and may be degraded or mistargeted (e.g. to mitochondria) due to the reduced number of import-competent peroxisomes (Ebberink et al. 2012).

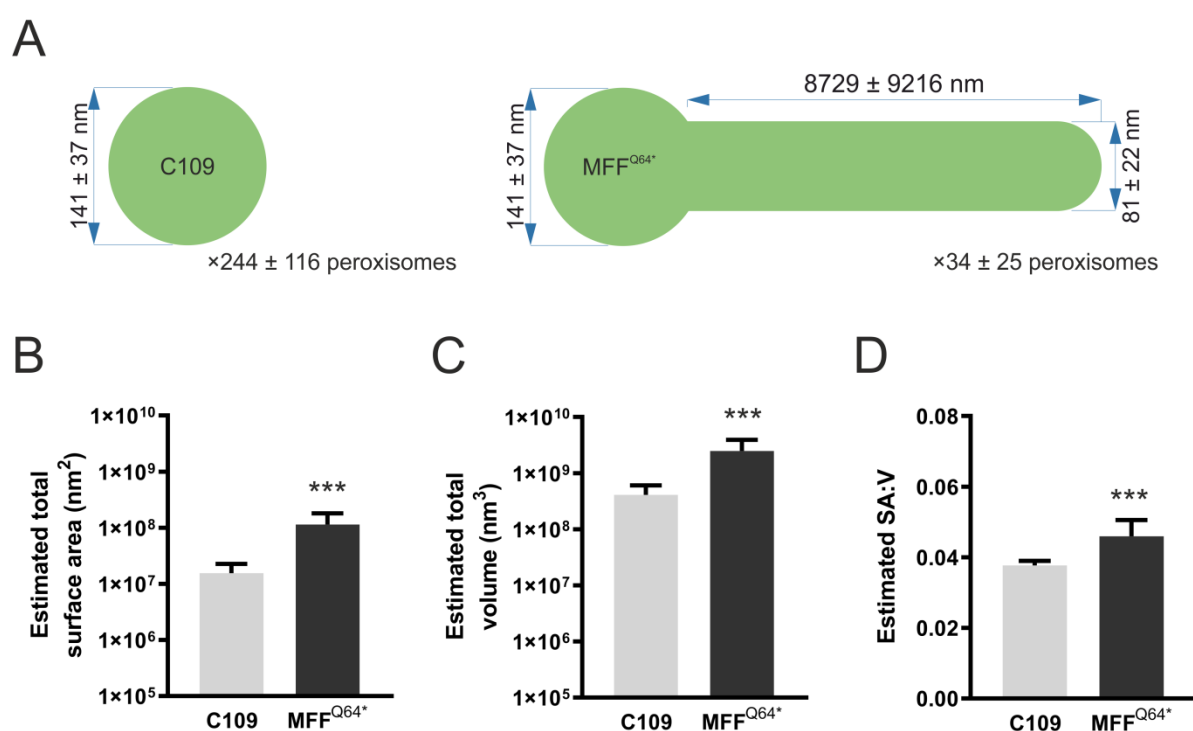




**Figure S1.** Calculations of peroxisomal surface area, volume, and surface area to volume ratio. **(A)** Values used for calculations (mean  $\pm$  SD). Control peroxisome body diameter was used as the calculated dMFF body diameter. **(B)** Estimated total peroxisomal surface area in control (CON) and MFF-deficient (dMFF) fibroblasts, based on an average of a computer-generated population of peroxisomes using values taken from the distributions shown in **(A)**. **(C)** Estimated total peroxisomal volume, and **(D)** estimated surface area to volume ratio (SA:V). Error bars show the mean + SD for 10,000 generated peroxisome populations. \*\*\*,  $P < 0.001$ ; two-tailed, unpaired t test.

We also show that peroxisomal matrix and membrane proteins do not distribute evenly along the elongated peroxisomes in MFF-deficient cells. Endogenous catalase or exogenously expressed GFP-SKL predominantly localise to the spherical body, whereas PEX14 localises predominantly to the tubular membrane extensions. A heterogeneous distribution of peroxisomal proteins during membrane growth and division has been reported previously (Delille et al. 2010; Cepińska et al. 2011). The specific mechanisms which restrict the mobility of the peroxisomal proteins and keep them within the spherical or tubular membrane domains are still unknown, but may depend on protein oligomerization and/or a specific lipid environment. However, the prominent localisation of PEX14, a component of the docking/translocation complex for matrix protein import, to the tubular peroxisomal membranes in MFF-deficient cells is unusual. It is possible that PEX14, which has been reported to interact with microtubules (Bharti et al. 2011; Theiss et al. 2012), may also act as a peroxisome-microtubule docking factor: it predominantly localises to the peroxisomal membrane extensions in MFF patient cells and may anchor them to microtubules in order to stabilise those highly elongated, delicate membrane structures and to facilitate membrane extension. The membrane topology of PEX14 is poorly defined, but a recent study suggested that the N-terminal domain is protease-protected and may not be exposed to the cytoplasm (Barros-Barbosa et al. 2019). Such a topology may be inconsistent with tubulin-binding, but it is possible that different populations or complexes of PEX14 exist which may fulfil different functions at the peroxisomal membrane.

Peroxisomes are oxidative organelles with important roles in cellular redox homeostasis (Fransen and Lismont 2018). Alterations in their redox metabolism have been suggested to contribute to aging and the development of chronic diseases such as neurodegeneration, diabetes, and cancer (Fransen and Lismont 2019). Using genetically encoded fluorescent sensors with ratiometric readout in live-cell approaches, we revealed alterations in the glutathione redox potential within peroxisomes of MFF-deficient fibroblasts, which was less oxidising compared to controls. Interestingly, in previous studies the intra-peroxisomal redox state in tubular peroxisomal compartments was also observed to be slightly lower than in spherical bodies (Lismont et al. 2017). In line with this, we also detected reduced levels of peroxisomal  $H_2O_2$  in MFF-deficient cells. The reason for this is unclear, but given that (i) peroxisome-derived  $H_2O_2$  can easily cross the peroxisomal membrane (Lismont et al. 2019a), and (ii) the surface to volume ratio is larger in the tubular structures, we hypothesize that  $H_2O_2$  can diffuse faster out of the tubular structures than out of the spherical bodies. Importantly, the glutathione redox balance and hydrogen peroxide levels in the cytosol and mitochondria were similar to controls, indicating peroxisome-specific alterations due to loss of MFF-function. Peroxisome-derived  $H_2O_2$  may be an important signalling messenger that controls cellular processes by modulating protein activity through cysteine oxidation (Fransen and Lismont 2019). However, the precise interrelationship between peroxisomal redox metabolism, cell signalling, and human disease remains to be elucidated. Further insight may come from the identification of primary targets for peroxisome-derived  $H_2O_2$ . We also revealed changes in the peroxisomal pH in MFF-deficient fibroblasts, which was more alkaline than in controls. The pI of most peroxisomal enzymes is basic, and consistent with this, an alkaline pH has been reported for the peroxisomal lumen (Dansen et al. 2000; van Roermund et al. 2004; Godinho and

Schrader 2017). Studies addressing peroxisomal pH under disease conditions are scarce, but a more acidic peroxisomal pH has been reported in fibroblasts from patients suffering from Rhizomelic Chondrodysplasia Punctata type 1, a PBD based on a defect in the import receptor PEX7 and impaired matrix protein import of PTS2-containing cargo (Dansen et al. 2000). It remains to be determined if those changes are the result of slightly altered metabolic activity and/or changes in membrane properties which impact on peroxisomal membrane channels/transporters. In line with this, calcium influx into peroxisomes has been reported to induce a minor increase of peroxisomal pH (Lasorsa et al. 2008). Whether peroxisomes possess a proton pump is still debated, but it has been suggested that a peroxisomal proton gradient may be needed to drive other transport processes across the peroxisomal membrane (Rottensteiner and Theodoulou 2006).

It is suggested that a block in peroxisome fission (e.g., due to mutations in MFF or DRP1), which results in the formation of larger, elongated organelles, may have deleterious effects on the mobility of peroxisomes, on synaptic homeostasis, and pexophagy (Schrader et al. 2014). We show here that highly elongated peroxisomes in MFF-deficient fibroblasts can be degraded by autophagic processes, which were induced by expression of a fragment of PEX3 [*HsPEX3*(1-44)] (Soukupova et al. 1999) or by amino acid starvation. Highly elongated mitochondria, for example, were reported to be spared from mitophagy under starvation conditions (Rambold et al. 2011; Gomes et al. 2011). Our data reveal that elongated peroxisomes are not spared from autophagic processes, e.g. due to physical limitations, and indicate that impaired peroxisome degradation may not contribute to the pathology of MFF-deficiency. Interestingly, a shortening of elongated peroxisomes was observed during amino acid starvation in HBSS, which was accompanied by a reduction in peroxisomal marker proteins, e.g. the PMPs ACBD5 and PEX11 $\beta$ , which are required for membrane expansion and elongation. PEX11 $\beta$  mediates membrane deformation and elongation of the peroxisomal membrane (Delille et al. 2010; Opaliński et al. 2011), whereas ACBD5 has recently been shown to mediate membrane contact sites between peroxisomes and the ER by interacting with ER-resident VAP proteins (Costello et al. 2017b; Hua et al. 2017). Depletion of ACBD5 (or VAP) in MFF-deficient fibroblasts resulted in a shortening of elongated peroxisomes, likely due to disruption of the peroxisome-ER contact sites and reduced transfer of lipids from the ER to peroxisomes, which are required for peroxisomal membrane expansion (Costello et al. 2017b; Schrader et al. 2019). Our findings are in line with these previous observations and indicate that elongated peroxisomes in MFF-deficient cells are not fully static, but still dynamic under certain conditions. It is possible that a shortening/fragmentation of elongated peroxisomes under conditions of amino acid starvation facilitates their subsequent removal by autophagy.

Mitochondrial and peroxisomal dynamics are particularly important for brain development and function (Berger et al. 2016; Khacho and Slack 2018), likely explaining why MFF-deficient patients show primarily neurological defects. In neuronal cells, there is a strict regulation of the size and number of mitochondria, with smaller, uniform mitochondria in the axon in contrast to longer, elongated mitochondria in the dendrites (Popov et al. 2005). In mice, this regulation of mitochondrial size in the axon has recently been reported to be dependent on MFF (Lewis et al. 2018). Importantly, loss of MFF did not significantly alter the mitochondrial membrane potential, ATP levels or the redox potential of the matrix, but was important for limiting presynaptic Ca<sup>2+</sup> dynamics, affecting neurotransmitter release, terminal axonal branching and circuit connectivity. We show here that depletion of MFF in primary mouse hippocampal neurons alters peroxisomal morphology and distribution. In contrast to fibroblasts, peroxisomes do not hyper-elongate, but appear enlarged and tend to cluster, affecting their uniform distribution within the soma. Neuronal peroxisomes preferentially accumulate in axon terminals during early postnatal development (Arnold and Holtzman 1978) but are virtually absent from the axon in mature projection neurons (Kassmann et al. 2011). Changes in ACBD5 expression have recently been

shown to alter peroxisome motility and distribution in mouse hippocampal neurons, but independent of the ACBD5-VAPB interaction (Wang et al. 2018). Neuronal peroxisomes are required for axonal integrity of Purkinje cells (De Munter et al. 2018), and peroxisomal ROS metabolism was reported to influence activities of pro-opiomelanocortin producing neurons in the hypothalamus (Diano et al. 2011) and synaptic transmission at neuromuscular junctions (Giniatullin et al. 2019) underlining the physiological importance of peroxisomes in neurons. It remains to be determined if the altered peroxisomal phenotype in neurons contributes to the neurological abnormalities observed in MFF-deficiency. However, loss of PEX11 $\beta$ , which is not a mitochondrial protein, also causes neurological abnormalities in patients and mouse models highlighting the importance of peroxisomal dynamics and plasticity in the brain (Li et al. 2002; Ebberink et al. 2012; Taylor et al. 2017).

In contrast to the more prevalent neurological features in human patients with MFF-deficiency, mice without MFF die of heart failure at week 13, as a result of severe cardiomyopathy, which is likely based on mitochondrial alterations (Chen et al. 2015). However, removal of MFF exacerbated neuronal loss, astrogliosis and neuroinflammation in a Huntington's disease mouse model (Cha et al. 2018). Similar to patient fibroblasts, peroxisomes (and mitochondria) in MFF-deficient mouse embryonic fibroblasts were highly elongated (Chen et al. 2015). Interestingly, peroxisomal length was not substantially altered in MFF-deficient mouse cardiomyocytes (Chen et al. 2015). This strongly indicates that peroxisome morphology and division is affected in a cell type-specific manner.

We recently developed a mathematical model to explain and predict alterations in peroxisome morphology and dynamics in health and disease conditions (Castro et al. 2018). In this stochastic, population-based modelling approach, each individual peroxisome consists of a spherical body with an optional cylindrical elongation. Peroxisome shape (i.e. the body radius and elongation length) are determined by (i) membrane lipid flow into the body (e.g., from the ER) (governed by rate  $\alpha$  and lipid flow constant  $\gamma$ ), (ii) elongation growth (governed by speed  $v$  and minimum body radius  $r_{min}$ ) and (iii) peroxisome division with a rate proportional to the elongation length (governed by rate  $\beta$  and minimum length  $L_{min}$ ). Peroxisome turnover is controlled by the peroxisome mean lifetime  $\tau$ . We recently demonstrated that this model is applicable to a range of experimental and disease conditions, e.g. loss of PEX5 in Zellweger spectrum disorders (Castro et al. 2018). With wild-type parameters, peroxisomes in the model are typically high in number, with only a low percentage showing elongations, all of which are short (**Fig. 7A**). The morphological alterations of peroxisomes in MFF-deficient fibroblasts that we have observed experimentally are captured by changing only one parameter, namely by reducing the division rate  $\beta$  to almost zero (**Fig. 7B**). As the membrane lipid flow rate and elongation growth speed remain unchanged, this results in reduced numbers of peroxisomes with significantly longer membrane elongations (**Fig. 7D, E**). The observation that control fibroblasts display large numbers of small, spherical peroxisomes, but turn into few, extremely elongated organelles upon blocking of peroxisomal division, indicates that membrane lipid flow rate, elongation growth speed and division rate must be high in fibroblasts under normal conditions. In contrast, low membrane lipid flow rate or elongation speed in other cell types may result in a population of small peroxisomes and reduced numbers. This is reflected by depletion of ACBD5, which impacts on peroxisome-ER tethering and membrane expansion, resulting in shorter peroxisomes in MFF-deficient cells (Costello et al. 2017b). This morphological change can also be captured in the model by reducing the lipid flow rate  $\alpha$  in addition to the division rate  $\beta$  (**Fig. 7C-E**). It is thus likely that peroxisome morphology is differently affected in various cell types in MFF-deficient patients. It should also be considered that environmental changes and related signalling events that trigger peroxisomal membrane expansion and division (e.g. metabolic alterations and certain stress conditions) can potentially promote the formation of hyper-elongated peroxisomes in formerly unaffected cell types and contribute to the pathophysiology of MFF-deficiency.

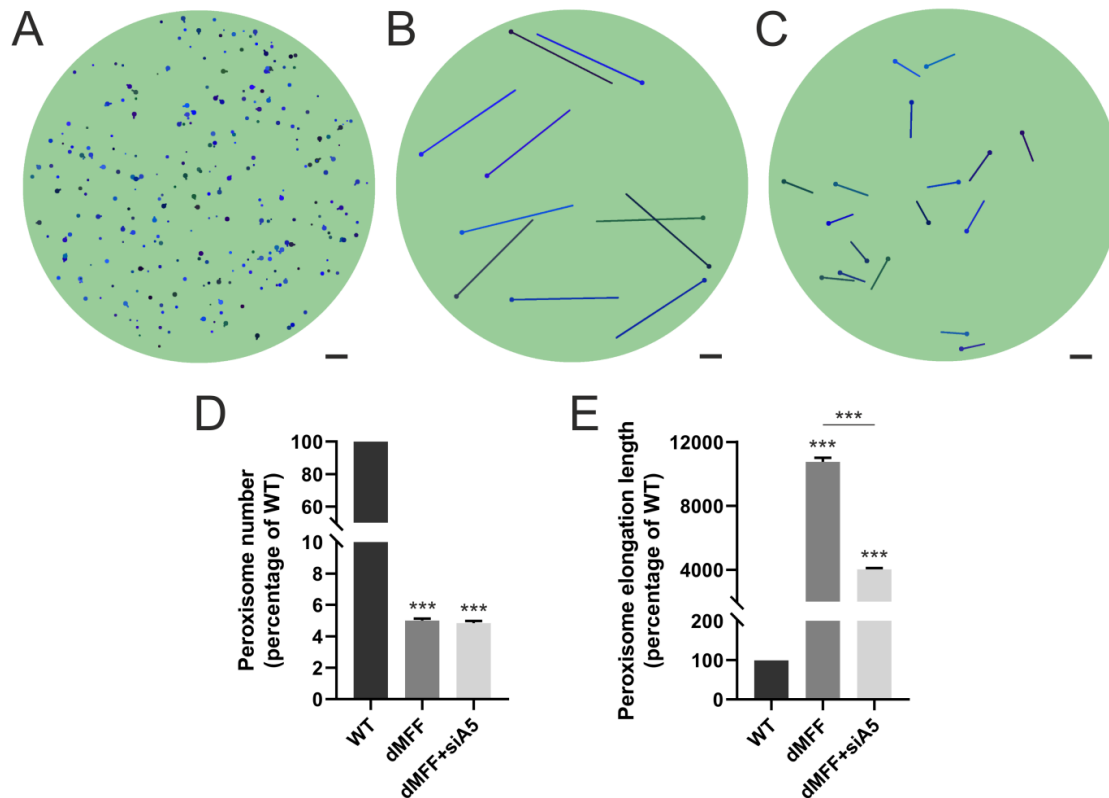


**Figure 7.** A mathematical model of peroxisome morphology and dynamics in wild-type and MFF-deficient patient fibroblasts. (A) Snapshot of model simulation for wild-type cells at  $t = 300$  hours ( $\alpha = 100 \text{ nm}^2/\text{s}$ ,  $\beta = 2 \times 10^{-5}/\text{nm/s}$ ,  $v = 0.3 \text{ nm/s}$ ,  $\tau = 4 \times 10^5 \text{ s}$ ,  $\gamma = 2.5 \times 10^{-7}/\text{nm}^2$ ). (B) Snapshot of model simulation of MFF-deficient cells (dMFF) at  $t = 300$  hours ( $\alpha = 100 \text{ nm}^2/\text{s}$ ,  $\beta = 2 \times 10^{-15}/\text{nm/s}$ ,  $v = 0.3 \text{ nm/s}$ ,  $\tau = 4 \times 10^5 \text{ s}$ ,  $\gamma = 2.5 \times 10^{-7}/\text{nm}^2$ ). (C) Snapshot of model simulation of MFF-deficient cells with reduced lipid flow to simulate silencing of ACBD5 (siA5) at  $t = 300$  hours ( $\alpha = 5 \text{ nm}^2/\text{s}$ ,  $\beta = 2 \times 10^{-15}/\text{nm/s}$ ,  $v = 0.3 \text{ nm/s}$ ,  $\tau = 4 \times 10^5 \text{ s}$ ,  $\gamma = 2.5 \times 10^{-7}/\text{nm}^2$ ). (D) Average peroxisome number at  $t = 300$  hours of simulations shown in A-C, represented as percentages relative to WT ( $n = 100$ ). (E) Average non-zero peroxisome elongation length at  $t = 300$  hours of simulations shown in A-C, represented as percentages relative to WT ( $n = 100$ ). Scale bars,  $10 \mu\text{m}$ .

## 5. Additional Information

### 5.1. Acknowledgements

We would like to thank F.S. Alkuraya, King Faisal Specialist Hospital and Research Center, Riyadh, Saudi Arabia for providing patient skin fibroblasts. This work was supported by BBSRC (BB/N01541X/1, BB/R016844/1; to M.S.), H2020-MSCA-ITN-2018 812968 PERICO (to M.S., M.F.), and the Research Foundation – Flanders (G095315N; to M.F.). M.I. was supported by the German Research Foundation (DFG Grant 397476530) and MEAMEDMA Anschubförderung, Medical Faculty Mannheim, University of Heidelberg. Y.W. was supported by the German Research Foundation (DFG Grant D10043030, SFB 1134 – Functional Ensembles). D.M.R. gratefully acknowledges financial support from the Medical Research Council (MR/P022405/1) and the Wellcome Trust Institutional Strategic Support Award (WT105618MA). C.L. was supported by the KU Leuven (PDM/18/188). Support grants to J.P. were provided by Zellweger UK, The Sidney Perry Foundation and The Devon Educational Trust.

The research data supporting this publication are provided within this paper and as supplementary information.

The authors declare no competing financial interests.

### 5.2. Author Contributions

JP, LG, SF, CL, YW, CH, MI, DR performed experiments and analysed data. MS, SF, PF, MF, MI conceived the project and analysed data. JP, MS wrote the manuscript. All authors contributed to methods.



## 6. References

- Anding AL, Baehrecke EH (2017) Cleaning House: Selective Autophagy of Organelles. *Dev Cell* 41:10–22. doi: 10.1016/j.devcel.2017.02.016
- Arias JA, Moser AB, Goldfischer SL (1985) Ultrastructural and cytochemical demonstration of peroxisomes in cultured fibroblasts from patients with peroxisomal deficiency disorders. *J Cell Biol* 100:1789–92
- Arnold G, Holtzman E (1978) Microperoxisomes in the central nervous system of the postnatal rat. *Brain Res* 155:1–17
- Asare A, Levorse J, Fuchs E (2017) Coupling organelle inheritance with mitosis to balance growth and differentiation. *Science* (80- ) 355:eaah4701. doi: 10.1126/science.aah4701
- Banker G, Goslin K, Stevens CF (1998) Culturing nerve cells. MIT Press
- Barros-Barbosa A, Ferreira MJ, Rodrigues TA, et al (2019) Membrane topologies of PEX13 and PEX14 provide new insights on the mechanism of protein import into peroxisomes. *FEBS J* 286:205–222. doi: 10.1111/febs.14697
- Berger J, Dorninger F, Forss-Petter S, Kunze M (2016) Peroxisomes in brain development and function. *Biochim Biophys Acta - Mol Cell Res* 1863:934–955. doi: 10.1016/j.bbamcr.2015.12.005
- Bharti P, Schliebs W, Schievelbusch T, et al (2011) PEX14 is required for microtubule-based peroxisome motility in human cells. *J Cell Sci* 124:1759–1768. doi: 10.1242/jcs.079368
- Bonekamp NA, Islinger M, Lázaro MG, Schrader M (2013) Cytochemical detection of peroxisomes and mitochondria. *Methods Mol Biol* 931:467–482. doi: 10.1007/978-1-62703-056-4\_24
- Braverman NE, Raymond G V, Rizzo WB, et al (2016) Peroxisome biogenesis disorders in the Zellweger spectrum: An overview of current diagnosis, clinical manifestations, and treatment guidelines. *Mol Genet Metab* 117:313–21. doi: 10.1016/j.ymgme.2015.12.009
- Brown L-A, Baker A (2008) Shuttles and cycles: transport of proteins into the peroxisome matrix (review). *Mol Membr Biol* 25:363–375. doi: 10.1080/09687680802130583
- Castro IG, Richards DM, Metz J, et al (2018) A role for Mitochondrial Rho GTPase 1 (MIRO1) in motility and membrane dynamics of peroxisomes. *Traffic* 19:229–242. doi: 10.1111/tra.12549
- Cepińska MN, Veenhuis M, van der Klei IJ, Nagotu S (2011) Peroxisome fission is associated with reorganization of specific membrane proteins. *Traffic* 12:925–37. doi: 10.1111/j.1600-0854.2011.01198.x
- Cha MY, Chen H, Chan D (2018) Removal of the Mitochondrial Fission Factor Mff Exacerbates Neuronal Loss and Neurological Phenotypes in a Huntington’s Disease Mouse Model. *PLoS Curr* 10:. doi: 10.1371/currents.hd.a4e15b80c4915c828d39754942c6631f
- Chen H, Ren S, Clish C, et al (2015) Titration of mitochondrial fusion rescues Mff-deficient cardiomyopathy. *J Cell Biol* 211:795–805. doi: 10.1083/jcb.201507035
- Costello JL, Castro IG, Camões F, et al (2017a) Predicting the targeting of tail-anchored proteins to subcellular compartments in mammalian cells. *J Cell Sci* 130:1675–1687. doi: 10.1242/jcs.200204
- Costello JL, Castro IG, Hacker C, et al (2017b) ACBD5 and VAPB mediate membrane associations between peroxisomes and the ER. *J Cell Biol* 216:331–342. doi: 10.1083/jcb.201607055



860 Costello JL, Passmore JB, Islinger M, Schrader M (2018) Multi-localized Proteins: The Peroxisome-  
861 Mitochondria Connection. In: Sub-cellular biochemistry. pp 383–415

862 Dacremont G, Cocquyt G, Vincent G (1995) Measurement of very long-chain fatty acids, phytanic  
863 and pristanic acid in plasma and cultured fibroblasts by gas chromatography. *J Inher Metab Dis*  
864 18 Suppl 1:76–83

865 Dansen TB, Wirtz KWA, Wanders RJA, Pap EHW (2000) Peroxisomes in human fibroblasts have a  
866 basic pH. *Nat Cell Biol* 2:51–53. doi: 10.1038/71375

867 De Munter S, Bamps D, Malheiro AR, et al (2018) Autonomous Purkinje cell axonal dystrophy  
868 causes ataxia in peroxisomal multifunctional protein-2 deficiency. *Brain Pathol*. doi:  
869 10.1111/bpa.12586

870 Delille HK, Agricola B, Guimaraes SC, et al (2010) Pex11p-mediated growth and division of  
871 mammalian peroxisomes follows a maturation pathway. *J Cell Sci* 123:2750–2762. doi:  
872 10.1242/jcs.062109

873 Diano S, Liu Z-W, Jeong JK, et al (2011) Peroxisome proliferation–associated control of reactive  
874 oxygen species sets melanocortin tone and feeding in diet-induced obesity. *Nat Med*. doi:  
875 10.1038/nm.2421

876 Dorninger F, Forss-Petter S, Berger J (2017) From peroxisomal disorders to common  
877 neurodegenerative diseases - the role of ether phospholipids in the nervous system. *FEBS Lett*  
878 591:2761–2788. doi: 10.1002/1873-3468.12788

879 Ebberink MS, Koster J, Visser G, et al (2012) A novel defect of peroxisome division due to a  
880 homozygous non-sense mutation in the PEX11 $\beta$  gene. *J. Med. Genet.* 49:307–313

881 Eberhart T, Kovacs WJ (2018) Pexophagy in yeast and mammals: an update on mysteries. *Histochem*  
882 *Cell Biol* 150:473–488. doi: 10.1007/s00418-018-1724-3

883 Ferdinandusse S, Ebberink MS, Vaz FM, et al (2016) The important role of biochemical and  
884 functional studies in the diagnostics of peroxisomal disorders. *J Inher Metab Dis* 39:531–543.  
885 doi: 10.1007/s10545-016-9922-4

886 Francisco T, Rodrigues TA, Dias AF, et al (2017) Protein transport into peroxisomes: Knowns and  
887 unknowns. *BioEssays* 39:1700047. doi: 10.1002/bies.201700047

888 Fransen M, Lismont C (2018) Peroxisomes and Cellular Oxidant/Antioxidant Balance: Protein Redox  
889 Modifications and Impact on Inter-organelle Communication. In: Sub-cellular biochemistry. pp  
890 435–461

891 Fransen M, Lismont C (2019) Redox Signaling from and to Peroxisomes: Progress, Challenges, and  
892 Prospects. *Antioxid Redox Signal* 30:95–112. doi: 10.1089/ars.2018.7515

893 Fransen M, Wylin T, Brees C, et al (2001) Human pex19p binds peroxisomal integral membrane  
894 proteins at regions distinct from their sorting sequences. *Mol Cell Biol* 21:4413–24. doi:  
895 10.1128/MCB.21.13.4413-4424.2001

896 Galiani S, Waithe D, Reglinski K, et al (2016) Super-resolution Microscopy Reveals  
897 Compartmentalization of Peroxisomal Membrane Proteins. *J Biol Chem* 291:16948–62. doi:  
898 10.1074/jbc.M116.734038

899 Gandre-Babbe S, van der Bliek AM (2008) The novel tail-anchored membrane protein Mff controls  
900 mitochondrial and peroxisomal fission in mammalian cells. *Mol Biol Cell* 19:2402–2412. doi:  
901 10.1091/mbc.E07

902 Gerber S, Charif M, Chevrollier A, et al (2017) Mutations in DNMI1L, as in OPA1, result in dominant  
903 optic atrophy despite opposite effects on mitochondrial fusion and fission. *Brain* 140:2586–2596.  
904 doi: 10.1093/brain/awx219

905 Giniatullin A, Petrov A, Giniatullin R (2019) Action of Hydrogen Peroxide on Synaptic Transmission  
906 at the Mouse Neuromuscular Junction. *Neuroscience* 399:135–145. doi:  
907 10.1016/j.neuroscience.2018.12.027

908 Godinho LF, Schrader M (2017) Determination of Peroxisomal pH in Living Mammalian Cells Using  
909 pHRed. In: *Methods in molecular biology* (Clifton, N.J.). pp 181–189

910 Gomes LC, Benedetto G Di, Scorrano L (2011) During autophagy mitochondria elongate, are spared  
911 from degradation and sustain cell viability. *Nat Cell Biol* 13:589–598. doi: 10.1038/ncb2220

912 Helle SCJ, Feng Q, Aebersold MJ, et al (2017) Mechanical force induces mitochondrial fission. *Elife*  
913 6:. doi: 10.7554/eLife.30292

914 Hua R, Cheng D, Coyaude É, et al (2017) VAPs and ACBD5 tether peroxisomes to the ER for  
915 peroxisome maintenance and lipid homeostasis. *J Cell Biol* 216:367–377. doi:  
916 10.1083/jcb.201608128

917 Huber N, Guimaraes S, Schrader M, et al (2013) Charcot-Marie-Tooth disease-associated mutants of  
918 GDAP1 dissociate its roles in peroxisomal and mitochondrial fission. *EMBO Rep* 14:545–552.  
919 doi: 10.1038/embor.2013.56

920 Itoyama A, Michiyuki S, Honsho M, et al (2013) Mff functions with Pex11p and DLP1 in  
921 peroxisomal fission. *Biol Open*. doi: 10.1242/bio.20135298

922 Ivashchenko O, Van Veldhoven PP, Brees C, et al (2011) Intraperoxisomal redox balance in  
923 mammalian cells: oxidative stress and interorganellar cross-talk. *Mol Biol Cell* 22:1440–1451.  
924 doi: 10.1091/mbc.E10-11-0919

925 Kassmann CM, Quintes S, Rietdorf J, et al (2011) A role for myelin-associated peroxisomes in  
926 maintaining paranodal loops and axonal integrity. *FEBS Lett* 585:2205–2211. doi:  
927 10.1016/j.febslet.2011.05.032

928 Kemp S, Valianpour F, Mooyer PAW, et al (2004) Method for measurement of peroxisomal very-  
929 long-chain fatty acid beta-oxidation in human skin fibroblasts using stable-isotope-labeled  
930 tetracosanoic acid. *Clin Chem* 50:1824–6. doi: 10.1373/clinchem.2004.038539

931 Khacho M, Slack RS (2018) Mitochondrial dynamics in the regulation of neurogenesis: From  
932 development to the adult brain. *Dev Dyn* 247:47–53. doi: 10.1002/dvdy.24538

933 Koch A, Schneider G, Lüers GH, Schrader M (2004) Peroxisome elongation and constriction but not  
934 fission can occur independently of dynamin-like protein 1. *J Cell Sci* 117:3995–4006. doi:  
935 10.1242/jcs.01268

936 Koch A, Yoon Y, Bonekamp NA, et al (2005) A Role for Fis1 in Both Mitochondrial and  
937 Peroxisomal Fission in Mammalian Cells. *Mol Biol Cell* 16:5077–5086. doi: 10.1091/mbc.E05

938 Koch J, Brocard C (2012) PEX11 proteins attract Mff and hFis1 to coordinate peroxisomal fission. *J*  
939 *Cell Sci* 125:3813–3826

940 Koch J, Feichtinger RG, Freisinger P, et al (2016) Disturbed mitochondrial and peroxisomal dynamics  
941 due to loss of MFF causes Leigh-like encephalopathy, optic atrophy and peripheral neuropathy.  
942 *J Med Genet* 53:270–278. doi: 10.1136/jmedgenet-2015-103500

943 Ladds E, Whitney A, Dombi E, et al (2018) De novo DNMI1L mutation associated with mitochondrial

944 epilepsy syndrome with fever sensitivity. *Neurol Genet* 4:e258. doi:  
945 10.1212/NXG.0000000000000258

946 Lasorsa FM, Pinton P, Palmieri L, et al (2008) Peroxisomes as novel players in cell calcium  
947 homeostasis. *J Biol Chem* 283:15300–15308. doi: 10.1074/jbc.M800648200

948 Lee MY, Sumpter R, Zou Z, et al (2017) Peroxisomal protein PEX13 functions in selective  
949 autophagy. *EMBO Rep* 18:48–60. doi: 10.15252/embr.201642443

950 Lewis TL, Kwon S-K, Lee A, et al (2018) MFF-dependent mitochondrial fission regulates presynaptic  
951 release and axon branching by limiting axonal mitochondria size. *Nat Commun* 9:5008. doi:  
952 10.1038/s41467-018-07416-2

953 Li X, Baumgart E, Morrell JC, et al (2002) PEX11 $\beta$  Deficiency Is Lethal and Impairs Neuronal  
954 Migration but Does Not Abrogate Peroxisome Function. *Mol Cell Biol* 22:4358–4365

955 Lismont C, Koster J, Provost S, et al (2019a) Deciphering the potential involvement of PXMP2 and  
956 PEX11B in hydrogen peroxide permeation across the peroxisomal membrane reveals a role for  
957 PEX11B in protein sorting. *Biochim Biophys Acta - Biomembr*. doi:  
958 10.1016/J.BBAMEM.2019.05.013

959 Lismont C, Nordgren M, Brees C, et al (2019b) Peroxisomes as Modulators of Cellular Protein Thiol  
960 Oxidation: A New Model System. *Antioxid Redox Signal* 30:22–39. doi: 10.1089/ars.2017.6997

961 Lismont C, Walton PA, Fransen M (2017) Quantitative Monitoring of Subcellular Redox Dynamics in  
962 Living Mammalian Cells Using RoGFP2-Based Probes. In: *Methods in molecular biology*  
963 (Clifton, N.J.). pp 151–164

964 Long B, Wang K, Li N, et al (2013) miR-761 regulates the mitochondrial network by targeting  
965 mitochondrial fission factor. *Free Radic Biol Med* 65:371–9. doi:  
966 10.1016/j.freeradbiomed.2013.07.009

967 Nasca A, Legati A, Baruffini E, et al (2016) Biallelic Mutations in DNM1L are Associated with a  
968 Slowly Progressive Infantile Encephalopathy. *Hum Mutat* 37:898–903. doi:  
969 10.1002/humu.23033

970 Nasca A, Nardecchia F, Commone A, et al (2018) Clinical and Biochemical Features in a Patient  
971 With Mitochondrial Fission Factor Gene Alteration. *Front Genet* 9:625. doi:  
972 10.3389/fgene.2018.00625

973 Ofman R, Wanders RJ (1994) Purification of peroxisomal acyl-CoA: dihydroxyacetonephosphate  
974 acyltransferase from human placenta. *Biochim Biophys Acta* 1206:27–34

975 Okumoto K, Ono T, Toyama R, et al (2018) New splicing variants of mitochondrial Rho GTPase-1  
976 (Miro1) transport peroxisomes. *J Cell Biol* 217:619–633. doi: 10.1083/jcb.201708122

977 Opaliński L, Kiel JAKW, Williams C, et al (2011) Membrane curvature during peroxisome fission  
978 requires Pex11. *EMBO J* 30:5–16

979 Palmer CS, Elgass KD, Parton RG, et al (2013) Adaptor proteins MiD49 and MiD51 can act  
980 independently of Mff and Fis1 in Drp1 recruitment and are specific for mitochondrial fission. *J*  
981 *Biol Chem* 288:27584–93. doi: 10.1074/jbc.M113.479873

982 Popov V, Medvedev NI, Davies HA, Stewart MG (2005) Mitochondria form a filamentous reticular  
983 network in hippocampal dendrites but are present as discrete bodies in axons: A three-  
984 dimensional ultrastructural study. *J Comp Neurol* 492:50–65. doi: 10.1002/cne.20682

985 Rambold AS, Kostecky B, Elia N, Lippincott-schwartz J (2011) Tubular network formation protects

986 mitochondria from autophagosomal degradation during nutrient starvation. *Proc Natl Acad Sci*  
987 U S A 108:10190–10195. doi: 10.1073/pnas.1107402108/-  
988 /DCSupplemental.www.pnas.org/cgi/doi/10.1073/pnas.1107402108

989 Raymond G V, Moser AB, Fatemi A (1993) X-Linked Adrenoleukodystrophy

990 Ribeiro D, Castro I, Fahimi HD, Schrader M (2012) Peroxisome morphology in pathology. *Histol*  
991 *Histopathol* 27:661–676

992 Rottensteiner H, Theodoulou FL (2006) The ins and outs of peroxisomes: Co-ordination of membrane  
993 transport and peroxisomal metabolism. *Biochim Biophys Acta (BBA)-Molecular Cell Res*  
994 1763:1527–1540. doi: 10.1016/j.bbamcr.2006.08.012

995 Sargent G, van Zutphen T, Shatseva T, et al (2016) PEX2 is the E3 ubiquitin ligase required for  
996 pexophagy during starvation. *J Cell Biol* 214:677–690. doi: 10.1083/jcb.201511034

997 Schneider CA, Rasband WS, Eliceiri KW (2012) NIH Image to ImageJ: 25 years of image analysis.  
998 *Nat Methods* 9:671–5

999 Schrader M, Bonekamp NA, Islinger M (2012) Fission and proliferation of peroxisomes. *Biochim*  
1000 *Biophys Acta - Mol Basis Dis* 1822:1343–1357. doi: 10.1016/j.bbadis.2011.12.014

1001 Schrader M, Castro I, Fahimi HD, Islinger M (2014) Peroxisome morphology in pathologies. In:  
1002 *Molecular Machines Involved in Peroxisome Biogenesis and Maintenance*. Springer, pp 125–  
1003 151

1004 Schrader M, Costello JL, Godinho LF, et al (2016) Proliferation and fission of peroxisomes - An  
1005 update. *Biochim Biophys Acta - Mol Cell Res* 1863:971–983. doi:  
1006 10.1016/j.bbamcr.2015.09.024

1007 Schrader M, Kamoshita M, Islinger M (2019) Organelle interplay-peroxisome interactions in health  
1008 and disease. *J Inherit Metab Dis*. doi: 10.1002/jimd.12083

1009 Schrader M, Thiemann M, Fahimi HD (2003) Peroxisomal Motility and Interaction With  
1010 Microtubules. *Microsc Res Tech* 61:171–178. doi: 10.1002/jemt.10326

1011 Schrader TA, Schrader M (2017) siRNA-mediated Silencing of Peroxisomal Genes in Mammalian  
1012 Cells. In: *Methods in molecular biology* (Clifton, N.J.). pp 69–79

1013 Shamseldin HE, Alshammari M, Al-Sheddi T, et al (2012) Genomic analysis of mitochondrial  
1014 diseases in a consanguineous population reveals novel candidate disease genes. *J Med Genet*  
1015 49:234–241. doi: 10.1136/jmedgenet-2012-100836

1016 Sheffer R, Douiev L, Edvardson S, et al (2016) Postnatal microcephaly and pain insensitivity due to a  
1017 de novo heterozygous DNM1L mutation causing impaired mitochondrial fission and function.  
1018 *Am J Med Genet A* 170:1603–7. doi: 10.1002/ajmg.a.37624

1019 Soliman K, Göttfert F, Rosewich H, et al (2018) Super-resolution imaging reveals the sub-diffraction  
1020 phenotype of Zellweger Syndrome ghosts and wild-type peroxisomes. *Sci Rep* 8:7809. doi:  
1021 10.1038/s41598-018-24119-2

1022 Soukupova M, Sprenger C, Gorgas K, et al (1999) Identification and characterization of the human  
1023 peroxin PEX3. *Eur J Cell Biol* 78:357–374. doi: 10.1016/S0171-9335(99)80078-8

1024 Sun M, Bernard LP, DiBona VL, et al (2013) Calcium Phosphate Transfection of Primary  
1025 Hippocampal Neurons. *J Vis Exp* e50808. doi: 10.3791/50808

1026 Tantama M, Hung YP, Yellen G (2011) Imaging Intracellular pH in Live Cells with a Genetically

1027 Encoded Red Fluorescent Protein Sensor. *J Am Chem Soc* 133:10034–10037. doi:  
1028 10.1021/ja202902d

1029 Taylor RL, Handley MT, Waller S, et al (2017) Novel PEX11B Mutations Extend the Peroxisome  
1030 Biogenesis Disorder 14B Phenotypic Spectrum and Underscore Congenital Cataract as an Early  
1031 Feature. *Invest Ophthalmol Vis Sci* 58:594–603. doi: 10.1167/iovs.16-21026

1032 Theiss C, Neuhaus A, Schliebs W, Erdmann R (2012) TubStain: a universal peptide-tool to label  
1033 microtubules. *Histochem Cell Biol* 138:531–540. doi: 10.1007/s00418-012-0992-6

1034 Thiemann M, Schrader M, Volkl A, et al (2000) Interaction of peroxisomes with microtubules In vitro  
1035 studies using a novel peroxisome-microtubule binding assay. *Eur J Biochem* 267:6264–6275

1036 van Roermund CWT, de Jong M, IJlst L, et al (2004) The peroxisomal lumen in *Saccharomyces*  
1037 *cerevisiae* is alkaline. *J Cell Sci* 117:4231–7. doi: 10.1242/jcs.01305

1038 Vanstone JR, Smith AM, McBride S, et al (2016) DNM1L-related mitochondrial fission defect  
1039 presenting as refractory epilepsy. *Eur J Hum Genet* 24:1084–1088. doi: 10.1038/ejhg.2015.243

1040 Wanders RJ, Denis S, Ruiters JP, et al (1995) Measurement of peroxisomal fatty acid beta-oxidation in  
1041 cultured human skin fibroblasts. *J Inher Metab Dis* 18 Suppl 1:113–24

1042 Wanders RJ, Van Roermund CW (1993) Studies on phytanic acid alpha-oxidation in rat liver and  
1043 cultured human skin fibroblasts. *Biochim Biophys Acta* 1167:345–50

1044 Wanders RJA (2018) Peroxisomal disorders: Improved laboratory diagnosis, new defects and the  
1045 complicated route to treatment. *Mol Cell Probes* 40:60–69. doi: 10.1016/j.mcp.2018.02.001

1046 Wang Y, Metz J, Costello JL, et al (2018) Intracellular redistribution of neuronal peroxisomes in  
1047 response to ACBD5 expression. *PLoS One* 13:e0209507. doi: 10.1371/journal.pone.0209507

1048 Waterham HR, Koster J, van Roermund CWT, et al (2007) A lethal defect of mitochondrial and  
1049 peroxisomal fission. *N Engl J Med* 356:1736–1741

1050 Williams C, Opalinski L, Landgraf C, et al (2015) The membrane remodeling protein Pex11p  
1051 activates the GTPase Dnm1p during peroxisomal fission. *Proc Natl Acad Sci U S A* 112:6377–  
1052 6382. doi: 10.1073/pnas.1418736112

1053 Yoon G, Malam Z, Paton T, et al (2016) Lethal Disorder of Mitochondrial Fission Caused by  
1054 Mutations in DNM1L. *J Pediatr* 171:313–316.e2. doi: 10.1016/j.jpeds.2015.12.060

1055